Accepted Manuscript

Geological Society, London, Special Publications

Early to Middle Ordovician sedimentation and bimodal volcanism at the margin of Iapetus: The Trollhøtta–Kinna basin of the Central Norwegian Caledonides

Bjørgunn H. Dalslåen, Deta Gasser, Tor Grenne, Lars E. Augland and Arild Andresen

DOI: https://doi.org/10.1144/SP503-2020-37

Received 21 February 2020
Revised 4 May 2020
Accepted 4 May 2020

Supplementary material at https://doi.org/10.6084/m9.figshare.c.4990752

Early to Middle Ordovician sedimentation and bimodal volcanism at the margin of Iapetus: The Trollhøtta–Kinna basin of the Central Norwegian Caledonides

Bjørgunn H. Dalslåen*[1]; Deta Gasser[2,3]; Tor Grenne[3]; Lars E. Augland[4, 1]; Arild Andresen[1]
[1]*Department of Geosciences, University of Oslo, Sem Sælands vei 1, 0371 Oslo, Norway*
[2]*Department of Environmental Sciences, Western Norway University of Applied Sciences, Røyrgata 6, 6856 Sogndal, Norway*
[3]*Geological Survey of Norway, Leiv Erikssons vei 39, 7040 Trondheim, Norway*
[4]*Centre for Earth Evolution and Dynamics, University of Oslo, Sem Sælands vei 1, 0371 Oslo*
* *Corresponding author: (b.h.dalslaen@geo.uio.no)*

Abbreviated title: The Ordovician Trollhøtta–Kinna basin

Abstract: The late Neoproterozoic to Palaeozoic Iapetus Ocean developed between Laurentia, Baltica, Siberia and Gondwana. Its Palaeozoic closure history is recorded by volcano-sedimentary successions within the Caledonian orogen of Scandinavia, the British Isles and Newfoundland. We present new lithological, geochemical and geochronological data relevant for the Iapetan closure history from the hitherto poorly known Trollhøtta–Kinna basin (central Norwegian Caledonides). This basin consists of alternating siliciclastic rocks, MORB, and felsic volcanic rocks highly enriched in e.g. Th, U and LREE. Rhyolites from the stratigraphically upper part are dated by zircon U-Pb TIMS to 473.3 ± 1.0 and 472.4 ± 0.7 Ma. Detrital zircon spectra indicate deposition after ~480 Ma, with sediments derived from composite Cambro-Ordovician and Archean to Neoproterozoic landmass(es), possibly the Laurentian margin or a related microcontinent. The peculiar bimodal volcanic association is interpreted as an intermittent phase of marginal basin rifting, derived from a heterogeneous mantle source previously metasomatized by continental material. The tectonic mechanisms behind rifting could be slab retreat and/or break-off, or far-field tectonic forces within the Iapetan realm. Comparison of this basin with other Iapetus-related, similarly-aged volcano-sedimentary successions along the Caledonian–Appalachian orogen indicate that the bimodal MORB and highly enriched rocks reflect a palaeotectonic setting hitherto unknown in the orogen.

Supplementary material: Analytical results for detrital zircon analyses.

The Iapetus Ocean is one of several oceanic basins which opened in the late Neoproterozoic and closed in the Palaeozoic, representing an important tectonic feature on the way from Pannotia to Pangea (e.g. Murphy et al. 2010; Nance & Murphy 2019). The existence of a Palaeozoic "proto-Atlantic" ocean, later termed Iapetus, was first proposed based on the rock record within the Scandinavian Caledonides, where faunas of similar age but with widely different provincialism are juxtaposed (Wilson 1966; Harland & Gayer 1972). Since then, remnants of this ocean have been documented all along the Caledonian orogen in the North Atlantic region, providing a gradually improving understanding of the opening and closure history of Iapetus (e.g. Neuman 1984; Pedersen et al. 1992; Harper et al. 1996; Mac Niocaill et al. 1997; Cawood et al. 2001; Murphy et al. 2010; van Staal et al. 2013; Waldron et al. 2014). Volcanic rocks and mafic dyke complexes indicate Late Neoproterozoic rifting of the ancient supercontinent, with subsequent break-up and separation of Baltica, Laurentia and Amazonia (which later became part of Gondwana) at around 620–550 Ma (e.g. Bingen et al. 1998; Cawood et al. 2001; Kjøll et al. 2019; Tegner et al. 2019), although the Late Neoproterozoic to Cambrian plate configuration prior to opening of Iapetus is still not fully resolved (e.g. Hartz & Torsvik 2002; Pisarevsky et al. 2008; Levashova et al. 2015; Torsvik & Cocks 2016; Nance & Murphy 2019).

Remnants of true mid-ocean ridge-related rocks from the Iapetan realm are not preserved; ophiolitic rocks within the Caledonian orogen mainly represent supra-subduction zone and island-arc settings related to the closing stages of Iapetus (Fig. 1a; e.g. Pedersen & Dunning 1997; Swinden et al. 1997; Hollis et al. 2013; Slagstad et al. 2014). The oldest supra-subduction zone rocks so far recognized within the Caledonian orogen indicate that outboard of the Laurentian and Gondwanan margins, subduction started at least by middle Cambrian times (ca. 510 Ma; e.g. van Staal et al. 2009; Zagorevski et al. 2010; Waldron et al. 2014; Domeier 2016). This marked the onset of a complex and long-lasting, Late Cambrian to Late Ordovician process of arc- and back-arc formation as well as accretion of arcs and microcontinents along the Laurentian margin, generally referred to as the Taconic Orogeny (e.g. van Staal et al. 2009). The various Taconic events are best documented within the northern Appalachians, but remnants of similar Late Cambrian to Late Ordovician tectonic events are known from the British Isles (e.g. Chew & Strachan 2014) and from allochthonous units within the Scandinavian Caledonides (Fig. 1; e.g. Pedersen et al. 1992; Yoshinobu et al. 2002; Roberts et al. 2007; Slagstad et al. 2011). The onset of Iapetus subduction along the Scandinavian margin of Baltica is less well constrained. Models depend on the palaeogeographic interpretation of subduction-related high-pressure rocks preserved within the allochthonous Seve Nappe Complex, which may be taken to indicate either onset of subduction outboard of Baltica in the early Ordovician (e.g. Gee et al. 2013), or a derivation of these high-pressure units from outboard Gondwana (e. g. Slagstad et al. 2020). The youngest ophiolitic rocks documented from the Iapetus realm are from a Late Ordovician (ca. 443 Ma) back-arc basin in the Scandinavian Caledonides (Furnes et al. 2012), and closure of the Iapetus Ocean is generally thought to have been completed by ca. 440–430 Ma (e.g. van Staal et al. 2009; Slagstad & Kirkland 2018).

Although the general narrative of this Cambrian to Silurian period of Iapetus closure is widely accepted, many details of the complex and at least 60 m.y. long series of accretionary events pertaining to the Taconic Orogeny are unknown. In particular, the Scandinavian Caledonides contain many Cambrian to Silurian volcano-sedimentary units with unknown eruptive and/or depositional age and poorly resolved geological history. In this contribution we present new field observations, geochemical data, and magmatic and detrital U–Pb zircon ages from the Trollhøtta unit of central

Norway (Figs. 1, 2). Our results show that this unit represents a marginal Early to Middle Ordovician (ca. 480–470 Ma) volcano-sedimentary basin with a highly peculiar bimodal volcanism not known from elsewhere in the Caledonian orogen of the North Atlantic region.

Geological setting

Iapetus-related units within the Scandinavian Caledonides

Rocks related to the Iapetus closure history occur all along the Scandinavian Caledonides, and are mainly assigned to the Köli nappe complex and correlatives, but also occur within the Helgeland and Seve nappe complexes (Fig. 1b; e.g. Gee et al. 1985; Corfu et al. 2014). Prominent rocks units derived from the Iapetus Ocean are the remnants of Late Cambrian to Early Ordovician supra-subduction zone ophiolites and primitive island arcs, such as from north to south the Lyngen Magmatic Complex (e.g. Selbekk et al. 1998; Augland et al. 2014), the Leka ophiolite (e.g. Pedersen & Furnes 1991), the Løkken–Vassfjellet–Bymarka (LVB) ophiolite fragments (e.g. Slagstad et al. 2014), the Fundsjø Group (Grenne & Lagerblad 1985) and the ophiolites and arc sequences at Gullfjellet, Bømlo/Stord and Karmøy (Fig. 1b; e.g. Dunning & Pedersen 1988; Pedersen & Dunning 1997). These units are overlain by various volcano-sedimentary successions of Early Ordovician to Silurian age. Relevant for our contribution are the Middle Ordovician Hovin Group of the western Trondheim region, including the Hølonda porphyrites, which overlies obducted and eroded LVB ophiolite fragments (Fig. 1b; e.g. Vogt 1945; Grenne & Roberts 1998), as well as the ca. 476–473 Ma basaltic to rhyolitic calc-alkaline Kattnakken and Siggjo volcanic rocks of southwestern Norway, which unconformably overlie the ophiolite fragments at Stord and Bømlo (Fig. 1b; Nordås et al. 1985; Pedersen & Dunning 1997). The Hølonda, Kattnakken and Siggjo volcanic rocks have been interpreted as representing continental arcs built upon ophiolites that were obducted onto the Laurentian margin or related continental fragments at ca. 475 Ma (Bruton & Bockelie 1980; Pedersen et al. 1992; Grenne & Roberts 1998; Slagstad et al. 2014).

Of interest with respect to the present study area is also the metabasaltic belt of the Støren Group *sensu stricto* (*s.s.*) of Grenne & Lagerblad (1985), Gee et al. (1985) and Stokke et al. (2018). This metabasaltic belt has traditionally been correlated with the LVB ophiolites (e.g. Wolff 1979; Nilsen & Wolff 1989). However, the Støren Group *s.s.* lacks gabbro and sheeted dyke complexes that characterize the latter units (Sturt et al. 1984; Furnes 1985; Gee et al. 1985), and it is characterised by MORB-type basalts, in contrast to the subduction signature of many LVB basalts (Grenne & Gasser 2017).

Iapetus-derived island arcs and oceanic basin-related units within the British–Irish Caledonides and Newfoundland

On the British Isles, island arc complexes and oceanic basins derived from the Iapetus Ocean are preserved mainly within the Midland Valley terrane, but the Cambrian to Ordovician rocks are poorly exposed due to extensive Late Ordovician to Silurian cover rocks. Two groups of Late Cambrian to Early Ordovician supra-subduction zone ophiolites and arc successions are known (Fig. 1c): the c. 503 Ma Strathy Complex (Fig. 1a; Dunk et al. 2019), the 500–490 Ma Unst, Highland Border, and Deer Park ophiolites, and the 490–480 Ma Ballantrae Ophiolite Complex and Tyrone Plutonic Group (490-

480 Ma; Fig. 1; e.g. Chew et al. 2010; Chew & Strachan 2014). In western Ireland, volcanic rocks overlying members of the first group of ophiolites are found as the ca. 490–467 Ma volcanic arc successions of the Bohaun, Lough Nafooey, Tourmakeady and Murrisk groups (Fig. 1c; Ryan et al. 1980; Clift & Ryan 1994; Chew et al. 2007). These arc sequences and their underlying 500–490 Ma ophiolites were subjected to arc-continent collision and obduction onto the Laurentian margin during the Grampian orogeny (Chew et al. 2007; Chew & Strachan 2014). In northeastern Ireland, the ca. 484–480 Ma ophiolitic Tyrone Plutonic Group was overthrust by the ca. 475–470 Ma Tyrone Volcanic Group, which is generally thought to represent a peri-Laurentian island arc/back-arc system that underwent several episodes of intra-arc rifting (Fig. 1c; e.g. Draut et al. 2009; Cooper et al. 2011; Hollis et al. 2012). Both the Tyrone Plutonic Group and the Tyrone Volcanic Group were probably accreted onto a peri-Laurentian continental block (the Tyrone Central Inlier) at ca. 470 Ma (e.g. Cooper et al. 2011; Chew & Strachan 2014).

In Newfoundland, three main supra-subduction zone belts (including ophiolites) are preserved (Fig. 1d): the Lushs Bight oceanic tract (510–500 Ma), the Baie Verte oceanic tract (490–483 Ma) and the Annieopsquotch accretionary tract (481-468 Ma; e.g. Dunning & Krogh 1985; van Staal et al. 2009; Zagorevski & Van Staal 2011). They occur within the Dunnage Zone, which also contains the remnants of a peri-Laurentian microcontinent (the Dashwoods block). The Lushs Bight oceanic tract was obducted onto the Dashwoods microcontinent during the Taconic 1 phase of van Staal et al. (2007). This was followed by subduction in the seaway between the Dashwoods and the Laurentian margin, which led to formation of the Baie Verte oceanic tract and the 488–435 Ma Notre Dame arc (Fig. 1d; e.g. Van Staal et al. 2007; van Staal et al. 2009). Accretion of Baie Verte oceanic tract, Notre Dame arc and Dashwoods to the Laurentian margin happened in the Taconic 2 phase (Van Staal et al. 2007), which is roughly equivalent to the Grampian orogeny in the British–Irish Caledonides. The Annieopsquotch accretionary tract formed over a W-dipping subduction zone in the Iapetus Ocean outboard of the Dashwoods–Notre Dame subzone, and consists of the ca. 481–478 Ma Annieopsquotch ophiolite belt, the Lloyds River ophiolite complex and the Buchan and Roberts Arm groups, all of which are ca. 473 Ma, and the ca. 468 Ma Otter Pond Complex (Lissenberg et al. 2005). The Annieopsquotch accretionary tract units were accreted onto the Dashwoods–Notre Dame subzone shortly after their formation (e.g. Zagorevski et al. 2006). Accretion within this system was still active around 462–464 Ma, when the complex was syn-kinematically intruded by the shoshonitic Portage Lake monzogabbro (Fig. 1d; Lissenberg et al. 2005).

Geology of the Oppdal area

The Oppdal area is located in the southwestern part of the Trondheim Nappe Complex, which belongs to the Köli Nappe Complex (Fig. 1b, Fig. 2). In the Oppdal area, the Trondheim Nappe Complex is preserved within a half-graben structure and separated from the underlying, higher grade nappes by the Vinstradalen fault (Fig. 2). The rocks of the Trondheim Nappe Complex are at greenschist facies, grading southwards into amphibolite facies close to the Vinstradalen fault. The area has been mapped by Rohr-Torp (1972) and Nilsen & Wolff (1989), who separated primarily metavolcanic rocks (metabasalts, tuffites, rhyolites and volcanic breccias) from metasedimentary rocks (greywackes and shales), inferring an unconformity between the two. Nilsen & Wolff (1989) correlated the metavolcanic rocks with the Støren Group and the metasedimentary rocks with the

Hovin Group to the north. Based on way-up criteria in pillow lavas and sandstones, Rohr-Torp (1972) postulated overturning and tight to isoclinal folding of the entire metavolcanic–metasedimentary succession in the northern part of the study area (Fig. 3a). Stokke et al. (2018) investigated parts of this succession in the Dugurdsknappen area (Fig. 2, Fig. 3a), describing an inverted and tightly folded succession of E-MORB basalts, chert, cherty siltstone and turbiditic sandstone, unconformably overlain by Silurian sandstones and calc-alkaline volcanic rocks. Recently, Dalslåen et al. (2020) separated rocks of the Oppdal area into the Trollhøtta, Skarvatnet and Skuggliberga units (Fig. 2) and investigated the volcanic rocks of the Skarvatnet unit in more detail. This unit consists of the Kinna volcanic succession, the Storgruvpiken rhyolite and the sedimentary Skaret succession. Zircon dating of a trachyte within the Kinna volcanic succession and the Storgruvpiken rhyolite gave Early to Middle Ordovician ages of 474 ± 1 Ma and 470 ± 1 Ma, respectively (Dalslåen et al. 2020).

We remapped large parts of the Trollhøtta unit in order to compare our results with previous work by Rohr-Torp (1972), Stokke et al. (2018) and Dalslåen et al. (2020). In the following, we present new field observations and interpretations focusing on the Gisnadalen–Dugurdsknappen and Stølen–Oppdal areas (Figs. 2, 3).

Gisnadalen–Dugurdsknappen area

The Gisnadalen–Dugurdsknappen area consists of bedded sand- and siltstones, intercalated with metabasaltic rocks, chert and local felsic volcanic rocks (Fig. 2, 3b). The section is cut by a major normal fault, where the eastern block has been down-faulted. East of this fault, the bedding dips moderately to steeply to the east. Graded sandstone beds are common (Fig. 4a) and indicate younging generally towards west (Fig. 3a). Locally, however, the bedding dips westwards and is graded up to the southeast, indicating local folding (Fig. 3a). In the following, we describe the section from the inferred stratigraphically lowermost part in the east, to the stratigraphically higher rocks in the west.

The stratigraphically lowermost part of the section starts with sandstones that are grey to greenish, fine- to coarse-grained and display graded beds (Fig. 4a) and local nodular calcareous concretions. The sandstones comprise predominantly detrital quartz (typically polycrystalline), K-feldspar, plagioclase and clasts of metabasaltic and felsic volcanic rocks (Fig. 4b). The matrix is dominated by epidote, fine-grained quartz and some carbonate. Two beds of metabasalt (<10 m thick) are found within this lowermost part of the succession (Fig. 3a).

The sandstone-dominated succession is overlain by a ca. 150 m thick metabasaltic unit, locally developed as pillow lava, which gives way upwards to beds of white or light grey ribbon chert and local red jasper. Further up, grey to greenish siltstones are intercalated with fine- to coarse-grained sandstones, followed by another 350–400 m thick, massive, non-pillowed fine- to medium-grained metabasaltic unit that represents either a series of sheet flows or doleritic sills. This unit is followed to the west by grey to greenish siltstones that are locally chlorite-rich and magnetite-bearing.

Further west, a stratigraphically higher, heterogeneous unit consists of thin metabasalt with lensoidal, pillow-like structures, overlain by a chlorite- and epidote-rich pillow breccia, which again is overlain by white to grey bedded chert. A conglomerate unit dominated by felsic volcanic clasts (Fig. 4c) overlies the chert. This is overlain by a heterogeneous succession of grey to greenish siltstones and silty chert (Fig. 4d), as well as medium to coarse grained sandstones with 1–3 m thick

conglomeratic beds. The conglomerates are dominated by felsic volcanic clasts, some up to 30 cm large, with minor mafic and intermediate volcanic clasts, as well as tonalite, chert, jasper and green siltstone clasts. Graded beds are common, consistently showing younging towards west (Fig. 3a). At the top of the heterogeneous succession, close to the major normal fault, there is a fine grained, pinkish, felsic volcanic rock (Figs. 2, 3) with a massive central part and angular fragments at the margin (Fig. 4e).

The rocks immediately west of the normal fault (Fig. 3b) are overturned to the west and tightly folded with generally steep easterly dip; even further west the overturned Trollhøtta units show more open folds. The succession comprises mostly metabasalts in northern parts of the investigated area (Fig. 2), while to the south metasedimentary rocks predominate and include green magnetite-bearing siltstones and subordinate sandstones. Locally well-preserved pillow lavas have 20–50 cm pillows with a chlorite rim and variolitic outer part; partially drained pillows with internal tabular lava shelves are also observed (Fig. 4f). Jasper or chert is commonly found overlying greenstone (Fig. 4g). Chert is commonly white to grey, but black, magnetite-bearing chert has also been observed (Fig. 4h). Locally there are thin conglomerate beds with carbonate-dominated clasts in a calcareous biotite-rich matrix. Felsic and intermediate extrusive rocks occur as narrow zones or lenses, often at the contact to or within ribbon chert (Fig. 2). These zones of volcanic rocks are usually less than 10 m thick, and several lenses seem to lie at the same stratigraphic level as semicontinuous zones. These felsic to intermediate extrusive rocks are light grey to pinkish, and are either very fine-grained and massive or have a fragmental structure consisting of mm- to cm-large whitish clasts in a darker matrix.

Stølen–Oppdal area

The succession of metasedimentary and metavolcanic rocks in the Stølen–Oppdal area is similar to that in the Gisnadalen–Dugurdsknappen area (Figs. 2, 3). The general orientation of the bedding turns from N–S strike with easterly dip in the Brattskarven area to E–W strike with northerly dip in the Stølen–Oppdal area (Fig. 2). The major normal fault from the Gisnadalen–Dugurdsknappen section continues southward and offsets the eastern part of the succession in the Skjørstadhovden area by ca. 300 m (Fig. 3). North of Stølen, a continuous section from the Innset massif to Oppdal centre is exposed, where sedimentary structures (graded beds) and pillow shapes of metabasaltic rocks suggest overturning of the beds and a younging direction towards the south. Bedding is generally steep in the Stølen area and flattens westwards towards Skjørstadhovden.

The succession in the Stølen–Oppdal area starts with grey to greenish silt- and sandstones. Local beds of conglomerate with elongate angular fragments of siltstone (possibly rip-up clasts), and sub-rounded to rounded fragments of felsic volcanic rocks, chert and quartz clasts are found within the siltstones. The sandstones are generally quartz-rich. One 5 m thick bed of white chert has been observed within this part of the succession. The silt-sandstone succession is stratigraphically overlain by grey chert (Fig. 5a) interbedded with siltstone, and gives way stratigraphically upwards to well preserved pillow lavas and pillow breccias. Pillows are up to 1 m across and locally have internal tabular shelves (Fig. 5b). Jasper beds occur locally at the contact between the pillow lava and the underlying white chert, and are most frequent in the area of Skjørstadhovden where pillow lava and chert alternate. Stratigraphically above the basaltic succession are greenish silt- and sandstones with graded beds (Fig. 5c). Granule conglomerate has been observed locally, comprising angular and

rounded fragments of greenstone, quartz (mainly polycrystalline quartz), felsic volcanic rocks, siltstone, jasper and smaller grains of K-feldspar and plagioclase (Fig. 5d).

Geochemistry

Methods

We analysed 31 samples from the Trollhøtta unit for major and trace elements, including twenty-seven that were classified as mafic and four as felsic based on field criteria. All samples were analysed at the Geological Survey of Norway, Trondheim. Major elements were analysed by X-ray fluorescence (XRF) spectrometry on glass beads fused with lithium tetraborate, and trace elements were analysed by XRF spectrometry on pressed powder. Rare Earth Elements (REE) and selected trace elements were analysed by inductively coupled plasma–mass spectrometry (LA-ICP–MS) on the glass bead used for XRF major element analysis. Common international standards were used for all methods. The results are reported in Table 1 and in Figs. 6 and 7.

Results

The bimodal SiO_2 composition of the Trollhøtta volcanic rocks is demonstrated by the TAS diagram (Fig. 6a). Nineteen samples plot in the field of basalt and eight in the fields of basaltic andesite and basaltic trachyandesite. The four felsic samples classify as trachyte/trachydacite or rhyolite. In the Nb/Y vs Zr/Ti diagram of Pearce (1996; Fig. 6b), which relies on immobile elements and avoids the uncertainty related to the mobile alkalis, all low-SiO_2 samples plot as basalt, suggesting some mis-classification in the TAS plot due to seafloor or metamorphic alteration of SiO_2 and/or alkalis. The four felsic samples plot within or close to the field of alkali rhyolite (Fig. 6b).

All mafic rocks fall within or close to the 'Mantle Array' field in the Th/Yb vs. Nb/Yb diagram of Pearce (2008), similar to mid-ocean ridge basalts (MORB, Fig. 6c). Based on the criteria of Gale et al. (2013) for subdivision of MORB into depleted, normal and enriched types (D-, N- and E-MORB, respectively), our 27 samples of mafic rocks can be separated into three groups; D-MORB type with chondrite-normalized $La/Sm < 0.8$ (6 samples), N-MORB type with La/Sm_N between 0.8 and 1.5 (18 samples), and E-MORB type with $La/Sm_N > 1.5$ (3 samples); this subdivision is also reflected in the Th/Yb vs. Nb/Yb diagram and overlaps with the range of N-MORB to E-MORB as defined by Pearce (2008).

N-MORB-normalized multi-element plots for the basaltic rocks (Figs. 7a and c) show a gradual change from depletion to enrichment of the most incompatible trace elements, with a gentle negative slope towards Th in D-MORB samples and a positive slope in E-MORB types. The D-MORB sample with the lowest trace element concentrations exhibits negative anomalies of Nb and Zr, but this is inconsistent with the lack of Ta and Hf anomalies and may be an artefact of analytical uncertainty at very low concentrations. Four samples have Pb peaks, but these are likely artefacts related to statistical uncertainty of data close to the detection limit of 5 ppm Pb, which is nearly ten times the normalizing value (0.55 ppm Pb; Gale et al. 2013). Many samples have U peaks, but the large variation from a marked relative enrichment (particularly in some D-MORB samples), to no U anomaly (in E-MORB samples that are most enriched in incompatible elements) indicates that the erratic positive U anomalies result from sea-floor alteration and are not primary magmatic. This is consistent with the well documented uptake and enrichment of U from seawater during sub-

seafloor metamorphism in modern settings (e.g. Dunk et al. 2002), a process that obviously has its strongest relative impact on normalised patterns of rocks like D-MORB with very low contents of other highly incompatible elements.

Chondrite-normalized patterns for the basaltic rocks (Figs. 7b and d) also show a gradual variation from depletion (in D-MORB) to enrichment (in E-MORB) of the most incompatible REE (La to Sm), along with a change from nearly flat to gently decreasing slopes from Sm to Lu, and La_N/Lu_N ratios of 0.43–3.49. Significant Eu anomalies are generally absent; very small negative anomalies, especially in samples with relatively low REE contents, and similarly small positive anomalies in a few samples with high REE, may be real but analytical artefacts cannot be excluded.

Trace element patterns of the alkaline felsic rocks differ strongly from those of the basaltic rocks. MORB-normalized patterns (Fig. 7e) all show extreme enrichments in Th–U and other highly incompatible elements (e.g., Th ≈ 300 x N-MORB, up to 105 ppm; Zr ≈ 10 x N-MORB, up to 1030 ppm). Moreover, they have large negative anomalies in Nb–Ta and minor, but analytically significant, positive Pb anomalies. All four samples have very steep REE patterns, with La_N/Lu_N around 60 and large negative Eu anomalies of ca. 0.3 (Fig. 7f). Two samples have a similar sloping pattern throughout the REE towards Lu, while the other two have steeper slopes through the light and middle REE and a nearly flat pattern from Ho to Lu, indicating that they belong to two slightly different geochemical groups.

U–Pb TIMS data

U–Pb methodology

Two of the felsic volcanic rocks were selected for zircon U–Pb TIMS dating (Fig. 2). Zircons were separated using standard magnetic and heavy liquid techniques. Zircons were examined and selected under a binocular microscope and subsequently chemically abraded (Mattinson 2005) by annealing for 3 days at 900 °C, and then partial dissolution in HF (+HNO_3) at 190 °C for ca. 14 hrs. The grains chosen for analysis were spiked with a mixed ^{202}Pb–^{205}Pb–^{235}U tracer that has recently been calibrated to the Earthtime (ET) 100 Ma solution (Ballo et al. 2019). After spiking, the zircons were dissolved in HF (+HNO_3) at ca. 195 ºC for 5 days in Krogh-type bombs (14BD_83) or at 210 ºC for >48 hrs in Parrish style micro capsules enclosed in a Parr bomb (15BD_828). Chemical separation of U and Pb (Krogh 1973) was done for all grains. Details of the mass spectrometric techniques and parameters used are given in Augland et al. (2010) and Ballo et al. (2019). The raw data were reduced using Tripoli (Bowring et al. 2011) and analytical errors and corrections (including Th corrections, assuming Th/U in the magma of 3) were incorporated and propagated using an Excel macro based on the algorithms of Schmitz and Schoene (2007). Ages were calculated using ISOPLOT (Ludwig 2003) and the decay constants of Jaffey et al. (1971).

Results

Sample 1 (14BD_83) is an alkali rhyolite from the top of the stratigraphic section east of the normal fault in the Gisnadalen–Dugurdsknappen area (Figs. 2, 4e). Five fragments of euhedral zircon prisms were analysed. The analyses are concordant to slightly discordant and the two youngest analyses are barely overlapping with the three oldest. Analyses no. 2 and 4 give the youngest $^{206}Pb/^{238}U$ ages, interpreted to reflect residual Pb-loss, and are thus omitted from the calculation of the mean age.

The weighted mean of the remaining three analyses gives a $^{206}Pb/^{238}U$ age of 472.4 ± 0.7 Ma (2σ; MSWD = 0.22) that we interpret as the emplacement age of the rock (Fig. 8a; Table 2). Alternatively, the two youngest analyses with an age of 469.7 ± 0.9 (2σ; MSWD = 0.001) could represent the age of the alkali rhyolite, in which case the three older analyses must represent antecrysts. However, given the high alkalinity of this rock it seems highly unlikely that antecrysts would remain undissolved throughout a long-lived magma history thus supporting the interpretation that the three oldest analyses represent the age of the rock and that the two youngest analyses reflect residual Pb-loss.

Sample 2 (15BD_828) is an alkali rhyolite from west of the normal fault close to Trollhøtta, which is intercalated with metabasaltic rocks (Fig. 2). Four euhedral, high aspect ratio zircons dominated by (110) crystal faces were analysed. All analyses are concordant and overlapping, and give a weighted mean $^{206}Pb/^{238}U$ age of 473.3 ± 1.0 Ma (2σ; MSWD = 0.87) that we interpret as the emplacement age of the rock (Fig. 8b; Table 2).

Detrital zircon data

Methods

Eight sandstone samples were selected for detrital zircon analysis (Fig. 2). The samples were processed at the University of Oslo and at the Geological Survey of Norway. They were crushed using standard methods and washed on a Wilfley table. Frantz magnetic separator was not used, as this can remove particular zircon populations from the sample (Sircombe & Stern 2002), but a hand magnet was used to remove strongly magnetic minerals. The zircons were separated by heavy liquids with a density of 2.80 ± 0.02 g/ml (samples 15BD_186, 15BD_202, 15BD_213 and 14BD_58) or 3.30 g/ml (samples TGR_201, TGR_199, 14BD_48 and 14BD_17). The separated grains were randomly picked, mounted in epoxy and examined with a combination of backscattered electron imaging and cathodoluminescence imaging prior to analysis. U–Pb analyses were carried out by LA–ICP–MS, using a Nu Plasma HR multicollector mass spectrometer equipped with Cetac LSX-213 G2+ laser microprobe at the Department of Geosciences, University of Oslo. U–Pb analyses follow the analytical protocols of Andersen et al. (2009). Ablation conditions were beam diameter 40 µm (aperture imaging mode), pulse frequency 10 Hz. An in-house spreadsheet was used for data reduction.

Only analyses with less than ± 10 % central discordance are included in the following descriptions and plots; for plots of the Caledonian population only analyses less than ±5% are included. For grains older than 1000 Ma the $^{207}Pb/^{206}Pb$ age is reported, while for grains younger than 1000 Ma the $^{206}Pb/^{238}U$ age is reported. All data are plotted as histograms with Kernel Density Estimates and cake plots in Fig. 9, and as upper quartile/lower quartile plots and cumulative distribution plots (Andersen et al. 2018) in Fig. 10.

No common lead corrections have been applied, but as a reasonable filter on common lead affected zircons, analyses with $^{206}Pb/^{204}Pb$ below 2000 were commonly discarded. We excluded 3–5 grains from each of the samples TGR210, TGR199, 14BD_48, 14BD_17, 15BD_186 and 15BD_213 on this criterion. However, samples 14BD_58 and 15BD_202 have anomalously low $^{206}Pb/^{204}Pb$ ratios

because of low recording of the ^{206}Pb signal during analysis, and the $^{206}Pb/^{204}Pb$ ratio >2000 criterion would have removed most of the dataset for these two samples. We compared the full set of analyses with a dataset where samples with $^{206}Pb/^{204}Pb$ ratio below 1000 had been removed to see if the curves and their uncertainties overlap in cumulative distribution plots. The curves representing the full and the filtered datasets, respectively, have overlapping uncertainties. We therefore consider the two samples with low ^{206}Pb signal to be reliable and these are reported with their full dataset. Analyses of standards were performed during the analytical runs and provide correct ages, which also indicate that the data are trustworthy. The full analytical data set can be found as Supplementary File 1.

Results

Gisnadalen–Dugurdsknappen area

We analysed five samples from the Gisnadalen–Dugurdsknappen section, which are in the following described from the stratigraphically oldest (easternmost) to the youngest (westernmost) sample (Figs. 2, 3). The zircons are commonly subrounded to rounded or fragments of larger grains; euhedral grains are rare.

Sample 15BD_186 is a coarse-grained grey sandstone with bluish quartz grains (Fig. 4b). Zircons are abundant. 136 grains were analysed, 91 of which were < 10% discordant. The youngest grain is 450 ± 5 Ma (0.0 % discordant), and the oldest grain is 3218 ± 15 Ma (6% discordant). The sample consists of 17% Ordovician to Cambrian grains (450–520 Ma), 48% Neo- to Palaeoproterozoic grains (800–2100 Ma) and 35% Archean grains (2300–3300 Ma, Fig. 9a). The Cambrian–Ordovician analyses are relatively spread, but with a cluster of four analyses at c. 510–520 Ma. The mean age of the youngest population (3 or more grains (< 5% discordant) with overlap in age at 2σ) is 508 Ma.

Sample 15BD_202 is a coarse-grained sandstone with abundant zircon. 147 grains were analysed, but only 76 grains were less than 10% discordant. The youngest grain is 472 ± 11 Ma (2% discordant) and the oldest grain is 2863 ± 16 Ma (–8.6% discordant). The sample consist of 12% Ordovician to Late Cambrian grains (460–500 Ma), 80% Neo- to Palaeoproterozoic grains (900–2000 Ma), and 6 % Archean grains (2600–2900Ma; Fig. 9b). The Cambrian–Ordovician analyses cluster around 480–490 Ma, with a mean age of the youngest population at 482 Ma.

Sample 15BD_213 is a sandstone with graded beds with abundant zircons. 142 grains were analysed, one run had poor analytical quality and has been excluded from the following. 83 of the remaining grains are < 10% discordant. The youngest grain is 478 ± 5 Ma (–3.7%) and the oldest grains are 3157 ± 14 and 3269 ± 17 Ma (–6.5% and –9.7% discordant, respectively). The sample consist of 12% Ordovician to Cambrian grains (460–510 Ma), 68% Neo- to Palaeoproterozoic grains (700–2200 Ma) and 18% Archean grains (2650–2750 Ma; Fig. 9c). The Cambrian–Ordovician analyses show a slight peak at 500–510 Ma. The mean age of the youngest population is 485 Ma.

14BD_17 is a coarse-grained sandstone. 99 zircons were analysed, 61 of these are < 10% discordant. The youngest grain is 492 ± 7 Ma (–2.1% discordant), and the oldest grain is 3201 ± 21 Ma. The sample consist of 39% Ordovician to Late Neoproterozoic grains (480–550 Ma), 49% Neo- to Palaeoproterozoic grains (900–2000 Ma), and 12% Archean grains (2500–3300 Ma; Fig. 9d). The Palaeozoic component shows a clear peak at 490–510 Ma, with two single analyses at 531 ± 6 and 551 ± 5 Ma. The mean age of the youngest population is 493 Ma.

14BD_58 is a medium- to coarse-grained sandstone with abundant zircons. 155 grains were analysed, 109 of which are < 10% discordant. The youngest concordant grain is 460 ± 5 Ma (–3.9 % discordant), the oldest is 2864 ± 20 Ma. The sample has 12% Ordovician to Cambrian grains (470–500 Ma), 73% Neo- to Palaeoproterozoic grains (900–2200 Ma) and 16% Palaeoproterozoic to Archean grains (2200–3000 Ma; Fig.9e). The Palaeozoic component shows a peak at 480–490 Ma, and the mean age of the youngest population is 477 Ma.

Stølen–Oppdal area

We analysed three samples from the Stølen–Oppdal area (Fig. 2). Two samples are from the Stølen section, stratigraphically below and above the chert–pillow lava succession (Fig. 2), whereas one sample is from Svarthaugen which is part of the stratigraphically younger Kinna volcanic succession of the Skarvatnet unit (Fig. 2). Zircon are commonly subrounded to rounded or fragmental; euhedral grains are rare.

Sample TGR_201 is a greyish immature greywacke/sandstone. 108 grains were analysed and 71 of these were < 10% discordant. The youngest grain is 487 ± 5 Ma (4.9% discordant) and the oldest is 3043 ± 28 Ma (–7.6% discordant). The sample has 22% Ordovician to Cambrian grains (470–530 Ma), 72% Neo- to Palaeoproterozoic grains (900–2200 Ma) and 6% Archean grains (2700–3100 Ma; Fig. 9f). The Palaeozoic component shows a broad peak between 480 and 510 Ma, the mean age of the youngest population is 491 Ma.

Sample TGR_199 is a coarse-grained sandstone with abundant zircons. 131 grains were analysed, out of these 105 grains were < 10% discordant. The youngest grain is 483 ± 3 Ma (1.1% discordant) and the oldest grain is 2993 ± 24 Ma (–6.6% discordant). The sample has 18% Ordovician to Cambrian grains (480–540 Ma), 72% Neo- to Palaeoproterozoic grains (900–2200 Ma) and 6% Early Palaeoproterozoic to Archean grains (2300–3000 Ma; Fig. 9g). The Palaeozoic component shows a major peak at 490–510 Ma, the mean age of the youngest population is 490 Ma.

Sample 14BD_48 is a sandy bed in a phyllite that is interpreted to belong to the Kinna volcanic succession of the Skarvatnet Unit. 83 grains were analysed, but only 59 were less than 10% discordant. The youngest grain is 468 ± 8 Ma (–3.7% discordant), the oldest grain is 2849 ± 15 Ma (–6.2% discordant). The sample has 17% Ordovician to Cambrian grains (460–510 Ma), 76% Neo- to Palaeoproterozoic grains (900–2300 Ma) and70% Early Palaeoproterozoic to Archean grains (2700–2900 Ma; Fig. 9h). The Palaeozoic component has no clear peak due to few analyses, the mean age of the youngest population is 473 Ma.

Discussion

The Trollhøtta–Kinna succession – a coherent late Early Ordovician volcano-sedimentary basin

Field relationships

Our field observations differ significantly from previous interpretations of Rohr-Torp (1972) and Nilsen & Wolff (1989), who inferred an unconformity between the volcanic rocks (metabasalts and

cherts), assigned by them to the Støren Group, and the turbiditic sand- and siltstones, assigned by them to the Hovin Group.

A key difference is the interpretation of the stratigraphy and structure in the Gisnadalen–Dugurdsknappen section (Fig. 3a). Rohr-Torp (1972) correlated the different basaltic units with each other and interpreted large-scale fold structures within the section (Fig. 3a). Our data demonstrate that the lithologies and stratigraphic relationships are not consistent with such a correlation, and way-up criteria indicate a general upwards succession towards the west (Fig. 3a). In addition, the sand- and siltstones between the doleritic unit and the normal fault are similar to the sand- and siltstones east of the doleritic unit, and have, according to our observations, no similarities to the Gula schists as suggested by Rohr-Torp (1972). Also, Rohr-Torp (1972) did not take the felsic volcanic rocks and the major unconformity below the Skuggliberga unit in the western part (Fig. 3a) into account in his correlations. The tight to isoclinal F2 fold documented by Stokke et al. (2018) in the Dugurdsknappen area is a relatively local feature just west of and in the footwall of the major normal fault (Fig. 3a), probably resulting from deformation related to the fault. Our observations therefore favour an interpretation of a generally continuous, overturned, westward-younging volcano-sedimentary succession in the Gisnadalen–Dugurdsknappen area (Fig. 3a).

Our field data also indicate that the uppermost part of the Trollhøtta succession passes laterally southwards into the Kinna volcanic succession (Dalslåen et al. 2020), since basaltic and sedimentary rocks of the Trollhøtta unit apparently interfinger with pyroclastic rocks of the Kinna volcanic succession southwest of the mountain Trollhøtta (Fig. 2). We therefore interpret the upper part of the Trollhøtta unit to be contemporaneous with the Kinna volcanic succession. This implies that the Trollhøtta and Kinna volcanic successions formed in the same depositional basin, here informally referred to as the Trollhøtta–Kinna basin.

Depositional age

The depositional age of the Trollhøtta–Kinna basin is constrained by U–Pb zircon TIMS ages from volcanic rocks in the upper part of the succession, and by the youngest detrital zircon ages from the sandstones. TIMS sample 1 is from the top of the Gisnadalen–Dugurdsknappen succession, giving a crystallisation age of 472.4 ± 0.7 Ma. Sample 2 is also from the upper part of the succession, and its 473.3 ± 1.0 Ma age overlaps with sample 1. This age is also within error of the 474 ± 1 Ma age of a trachyte from the Kinna volcanic succession (Dalslåen et al., 2020), which we interpret as being coeval with the upper part of the Trollhøtta unit. These three ages therefore provide a robust constraint on the depositional age of the upper part of the Trollhøtta–Kinna basin. Sedimentation and volcanism may have continued for some time after 472 Ma. The timing is apparently limited by the 470 Ma Storgruvpiken rhyolite, which intrudes the Kinna volcanic succession (Dalslåen et al. 2020); however, we cannot exclude the possibility that Kinna–Trollhøtta volcanism and sedimentation resumed and continued after formation of the Storgruvpiken rhyolite.

The onset of deposition and volcanism is more loosely constrained, as no dateable felsic volcanic rocks have been found in the lower part of the succession. Maximum depositional ages can be calculated from youngest detrital zircon grains. It is generally accepted that the mean age of the youngest three or more grains that overlap in age at 2σ may provide a statistically robust estimate for the maximum depositional age of a sample (Dickinson & Gehrels 2009). With this approach, our eight samples indicate maximum depositional ages in the range of 473 to 508 Ma. Together with the

general Palaeozoic detrital peaks in the age range 480–510 Ma and the zircon ages of volcanic rocks, this suggests that deposition in the Trollhøtta–Kinna basin started later than ca. 480 Ma and continued at least to ca. 472 Ma.

The youngest detrital zircons from sample 15BD_186 deserve a few additional comments. This sample has four detrital zircon grains < 5% discordant at 450–470 Ma; 450 ± 5 Ma (0.1% discordant), 452 ± 4 Ma (-3.6% discordant), 465 ± 5 Ma (-3% discordant) and 470 ± 7 Ma (1.6% discordant). With less rigorous approaches to maximum depositional age calculations (youngest and oldest grain in the population overlap with the grains in between, but not each other), these grains could be used to derive a maximum depositional age for this sample of ca. 460 Ma. This young age would obviously be in conflict with the interpretation that this sample is from the base of a volcano-sedimentary succession, older than the overlying 473-474 Ma volcanic rocks. Uncritically, these grains could be used to argue for the following models: 1) the stratigraphic interpretation is wrong and the youngest rocks occur in the eastern part of the section, although way up criteria are consistent through the exposed part of the section, or 2) the Gisnadalen section consists of two separate extensional basins, one older basin in the west, including the 473 Ma volcanic rocks, and one basin younger than c. 450 Ma in the east, with an out-of-sequence thrust in between. We consider both models as highly speculative, being based solely on the presence of four young zircon grains in only one of the eight samples, when no other evidence supports such interpretations. Rather, we suggest that these young zircons were partially reset by the intrusion of the c. 435 Ma Innset diorite–trondhjemite massif (Nilsen et al. 2003), which is relatively close (less than 700 m) to the sample locality. Similar alteration of zircons by heating or interaction with magmatic fluids has been described e.g. from the Dalradian Supergroup in Shetland (Strachan et al. 2013) and from the Gardar Province in Greenland (Andersen 2013).

Source areas

The age distribution of the detrital zircons within the siliciclastic rocks also tells us something about the nature of the source area. Three main age groups were observed in the detrital zircon data: Palaeozoic (mainly 480–510 Ma), Proterozoic (mainly 900–2100 Ma) and Paleoproterozoic to Archean (2200–3300 Ma; Figs. 9, 10). The proportions of these age groups vary between the samples, with sample 14BD_17 (39% Palaeozoic grains) and sample 15BD_186 (35% Archean grains) representing endmembers of an otherwise relatively similar zircon distribution (Figs. 9, 10). We could not identify any systematic variation of the different age groups through the stratigraphy (Fig. 9).

The sources for the Palaeozoic (480–510 Ma) grains are most probably supra-subduction zone ophiolites and early island arcs from the Iapetan realm, which have contributed up to 40% of the analysed zircons to the Trollhøtta–Kinna basin. This suggests that the ophiolites and/or island arcs were exposed to erosion at the time of Trollhøtta–Kinna deposition, and that there were no sediment traps (such as island arcs or trenches) between the source area and the depositional basin. The LVB ophiolites and the Fundsjø Group are the closest remnants of such rocks in the central Caledonides (Fig. 1b). The LVB ophiolites were obviously eroded prior to deposition of the Hovin Group (e.g. Vogt 1945), inferably after obduction on a continental landmass (microcontinent or continental margin) in the Peri-Laurentian realm (e.g. Bruton & Bockelie 1980; Grenne & Roberts

1998; Slagstad et al. 2014). The Proterozoic and Archean detrital grains must be sourced from the same landmass, and (polyphase) recycling from younger successions have to be taken into account.

It is now generally recognised that the continental landmasses of Laurentia and Baltica have rather similar detrital zircon signatures, making it difficult to use detrital zircons as definite provenance indicators for either Laurentia or Baltica (e.g. Slagstad & Kirkland 2017). However, the large number of Archean grains and the age distribution in our samples may support more a Laurentian affinity, with the Archean craton of Greenland as a potential source. In contrast to the Archean of Greenland, 2.75–2.65 Ga igneous rocks are abundant in the Archean of Baltica (Hölttä et al. 2008). This is an age range that is poorly represented in our samples (Figs. 9, 10). On this basis, together with the possible paleogeographic link to the Hølonda terrane further north where Laurentian faunas prevail (e.g. Bruton and Bockelie, 1980), we speculate that the Trollhøtta–Kinna basin formed adjacent to the Laurentian margin or a related microcontinent.

Volcanic setting: bimodal MORB and extremely enriched felsic volcanism

A highly heterogenous mantle source

The rocks of the Trollhøtta–Kinna basin reflect several periods of volcanic activity within a dominantly siliciclastic basin. All our basaltic rocks have MORB-like trace element patterns, the majority being similar to typical N-MORB compositions, suggesting that they formed from a normal mantle source (e.g. Gale et al., 2013). Although basaltic rocks are by far predominant in the Trollhøtta succession, the volcanic rocks are strikingly bimodal, with broadly coeval deposition of the mafic and local felsic varieties. The association of MORB-type basaltic rocks and extremely enriched felsic rocks is unusual and provides some possible constraints on palaeotectonic models. The felsic rocks, although volumetrically subordinate, are particularly intriguing by virtue of their extreme geochemical compositions. Having trace element patterns and ratios highly contrasting with those of the associated basaltic rocks, a relationship to a common parental magma can obviously be disregarded.

The Trollhøtta felsic rocks share many of their peculiar geochemical traits with the Kinna volcanic succession (Fig. 7e, f; Dalslåen et al., 2020), with which the Trollhøtta succession interfingers in its upper part, as well as with the Storgruvpiken rhyolite that is associated with the Kinna volcanic succession. Notably, all these rocks are exceptionally enriched in highly incompatible trace elements, e.g. Th, U, and LREE. The exceptional composition of these rocks was discussed in detail by Dalslåen et al. (2020), who concluded that the enrichment in highly incompatible elements is too extreme to have resulted from fractional crystallization of normal mantle-derived magma, even if extensive crustal assimilation occurred. Instead, the Kinna volcanic succession was interpreted as being derived from a mantle source strongly modified by metasomatism from partial melts of subducted, continent-derived material (continental crust and/or continent-derived sediments). Partial melting of variably metasomatized mantle domains then produced the highly enriched Kinna group 1–3 magma series. The variation from mafic through intermediate to felsic compositions within the Kinna groups was interpreted to result largely from fractional crystallisation, whereas the uniformly rhyolitic Storgruvpiken magma apparently requires a more complex model including remelting of Kinna-type intrusions at lower crustal levels (Dalslåen et al., 2020).

In detail, the Trollhøtta felsic volcanic rocks show two distinctly different trace element patterns, none of which directly overlaps with any of the Kinna–Storgruvpiken volcanic rocks. In particular, the Trollhøtta felsic rocks lack the pronounced beryllium anomaly typical of Storgruvpiken and Kinna groups 2 and 3, and positive Pb anomalies are also significantly less distinctive. Moreover, Trollhøtta felsic volcanic rocks are even more enriched in REE (Fig. 7e–f). Notably, both types of Trollhøtta felsic volcanic rocks have REE patterns distinctly different from those of the geochemically homogeneous Storgruvpiken rhyolite. Furthermore, two of the Trollhøtta felsic rocks (green symbols) have REE and MORB-normalised geochemical patterns virtually parallel to, but at somewhat higher concentrations than, those of Kinna group 1 (Fig. 7e, f), implying that they could represent a more fractionated and felsic variety of the Kinna group 1 series. The other two Trollhøtta felsic samples (red symbols) exhibit some similarity to the Kinna group 2 series and might also be interpreted as fractional crystallisation products of mafic or intermediate melts, although directly relatable Kinna-type volcanic rocks remain to be documented.

The coexistence of MORB-type basaltic and extremely enriched felsic volcanic rocks in the Trollhøtta basin implies that the mantle source below this basin was extremely heterogeneous, with highly metasomatized mantle domains adjacent to pristine, unaltered asthenospheric mantle. This would be in accordance with the model of Foley (1992), who suggested that mantle metasomatism may produce distinct networks of altered veins consisting of clinopyroxene and mica between unaltered peridotite (see also Spandler & Pirard 2013; Förster et al. 2017). In such a scenario, both veins and unaltered peridotite domains could be tapped during separate but near-contemporaneous melting events, producing the extremely contrasting volcanic rocks of the Trollhøtta–Kinna basin.

Possible palaeotectonic scenarios

The model for the extremely enriched felsic rocks presented above apparently requires formation of these rocks above a “dying” subduction zone after arc–continent collision, probably along the Laurentian margin or a related microcontinent (Dalslåen et al. 2020). However, the MORB-related basaltic rocks also require a certain amount of rifting. We envisage two different tectonic scenarios that could be responsible for the rifting and MORB formation within such a setting.

(1) The Trollhøtta–Kinna rifting and basin formation could be directly related to the tectonic situation along the Laurentian margin or a related microcontinent after the arc–continent collision leading to the obduction of the LVB ophiolite. Comparing the Kinna–Storgruvpiken rocks with the broadly contemporaneous shoshonitic Hølonda Porphyrites further north, Dalslåen et al. (2020) suggested that the latter were derived from a heterogeneously metasomatized mantle comparable to that envisaged for the Trollhøtta–Kinna basin, although with less-metasomatized mantle domains or larger amounts of wall-rock versus vein-derived mantle melts. If correct, this would link the Trollhøtta–Kinna basin to the classical Hølonda terrane. Presupposing a palaeogeographic link between the Trollhøtta–Kinna successions and the Hølonda–LVB ophiolite terrane, rifting could have formed in response to collision of the LVB ophiolite–arc system with a continental margin on the Laurentian side of Iapetus. In such a scenario, LVB obduction may have been followed by steepening and ultimately detachment of the inferably east-dipping oceanic slab, possibly leading to subsidence and rifting in the overriding oceanic plate. In such dynamic settings different mantle sources are likely to be juxtaposed, potentially producing magmas with contrasting geochemical characteristics. However, we could not find any similar record of MORB-type volcanism in a marginal basin from

more modern arc–continent collisions followed by slab breakoff, so we are not sure whether this could be a feasible tectonic mechanism.

(2) The Trollhøtta–Kinna rifting could have been caused by far-field tectonic forces, related either to large-scale plate reorganization within the wider Laurentia–Baltica–Gondwana system that led to a short-lived true extensional phase along the Laurentian margin, or related to more local stress perturbations along an embayed Laurentian margin that lead to local extensional or transtensional rifting. Discriminating between the two different models is currently difficult due to uncertainties in plate tectonic reconstructions, both with regards to the palaeogeographic position of the Trollhøtta–Kinna basin during its formation, the age and palaeotectonic setting of adjacent units such as the Gula Complex and the Fundsjø Group and related rocks, and the number and polarity of subduction zones within Iapetus in Middle Ordovician times.

The Trollhøtta–Kinna basin – a unique feature within the Caledonides?

The Trollhøtta–Kinna basin represents a peculiar Early to Middle Ordovician volcano–sedimentary basin hitherto unknown in the central Scandinavian Caledonides. Based on lithological and geochemical similarities, Stokke et al. (2018) suggested a link between the Trollhøtta succession at Dugurdsknappen and the Støren Group *s.s.* further north, which would then extend the along-strike length of Trollhøtta–Kinna-type basinal deposits to at least 120 km. The similarities of the Kinna–Storgruvpiken volcanic rocks with the broadly contemporaneous shoshonitic Hølonda Porphyrites further north, as suggested by Dalslåen et al. (2020), may also link the Trollhøtta–Kinna basin to the classical Hølonda terrane further north, indicating a possible peri-Laurentian origin of this basin system.

Bimodal volcano–sedimentary successions of this age with similarly enriched felsic volcanic rocks and coeval MORB have not been documented elsewhere along the Caledonian orogen. The Trollhøtta basin overlaps in age with the basaltic to rhyolitic Kattnakken and Siggjo volcanic rocks in SW Norway, but the basaltic rocks of the Siggjo Complex show a clear subduction-zone signature and are interpreted to represent continental arc rocks (Pedersen & Dunning 1997; Viken 2017).

Within the Caledonides of the British Isles, only the rocks of the Tyrone Volcanic Group and the Tourmakeady and Murrisk groups in Ireland overlap in age with the Trollhøtta–Kinna basin (Fig. 1c; e.g. Clift & Ryan 1994; Cooper et al. 2011; Hollis et al. 2012). The Tyrone Volcanic Group consists of mafic to intermediate pillow lavas, volcaniclastic tuffs, rhyolites, banded chert, silica–iron exhalite (ironstone) and argillaceous sediment (Cooper et al. 2011), resembling to some degree the chert–volcanite parts of the Trollhøtta unit. A rhyolite in the upper part of the group is dated at 473±1 Ma (Cooper et al. 2008), identical to our reported age from the upper Trollhøtta basin. Interestingly, the Tyrone Volcanic Group shows an association of LILE- and LREE-enriched island-arc volcanic rocks with E-MORB compositions and LREE-depleted island-arc tholeiites (IAT) compositions, indicating a complex interplay between arc- and rift-related processes (Hollis et al. 2012). However, the enriched rocks in the Tyrone Volcanic Group are far less enriched than the Trollhøtta rocks (Draut et al. 2009; Cooper et al. 2011; Hollis et al. 2012), making a direct correlation or a similar tectonic setting of the Trollhøtta–Kinna basin with the Tyrone Volcanic Group unlikely. Similarly, the felsic volcanic rocks in the Tourmakeady and Murrisk groups of the South Mayo Through are also far less enriched in LREE

than the Trollhøtta volcanic rocks, and they are not associated with MORB-type basalts (Clift & Ryan 1994).

On Newfoundland, rocks of similar age are present within the Annieopsquotch accretionary tract: the ca. 473 Ma Lloyds River ophiolite complex and the ca. 473 Ma Buchan and Roberts Arm Groups (Fig. 1d; e.g. Lissenberg et al. 2005; Zagorevski et al. 2006). The Lloyds River ophiolite complex contains both MORB-like rocks and rocks enriched in Th and LREE (but again far below the Trollhøtta enrichments) interpreted as having formed in a wide back-arc basin related to an additional west-dipping subduction zone between the accreted Dashwoods microcontinent and Ganderia (Zagorevski & Van Staal 2011). However, the Lloyds River ophiolite complex is sediment-starved and not associated with siliciclastic rocks such as in the Trollhøtta–Kinna basin.

Interestingly, the Annieopsquotch accretionary tract is stitched by the shoshonitic 462–464 Ma Portage Lake monzogabbro, which shows the most incompatible element-enriched compositions of coeval Caledonian magmatic rocks. It shows enrichments on the order of Kinna group 1 (the least-enriched Kinna rocks), comparable to the shoshonitic Hølonda Porphyrites (Grenne & Roberts 1998; Lissenberg et al. 2005; Dalslåen et al. 2020). The Portage Lake monzogabbro is interpreted to represent melting of sub-arc mantle during slab breakoff from the subduction zone which closed the Humber Seaway during the Grampian Orogeny (e.g. Lissenberg et al. 2005; Zagorevski & Van Staal 2011), a model similar to our petrogenetic model for the Kinna and Trollhøtta felsic volcanic rocks and the Hølonda porphyrites.

Conclusions

The Trollhøtta succession is part of a coherent, Early to Middle Ordovician (ca. 480–470 Ma) volcano-sedimentary basin, here informally termed the Trollhøtta–Kinna basin, which probably was deposited along the Laurentian margin or an associated microcontinent. The Trollhøtta-Kinna basin represents a hitherto poorly documented volcano-sedimentary phase within the Trondheim Nappe Complex of the Scandinavian Caledonides. The Trollhøtta succession is dominated by turbiditic, siliciclastic sediments derived from a composite Cambro–Ordovician and Proterozoic to Archean landmass, requiring a complex, subaerially exposed source region that included both ancient continental crust and Palaeozoic rocks, the latter inferred to be obducted supra-subduction zone ophiolites and/or island arcs. The Trollhøtta succession also contains a peculiar association of D-, N- and E-MORB basalts along with felsic lavas extremely enriched in for instance Th, U and LREE, requiring an extremely heterogeneous mantle source. The enriched felsic rocks are related to the coeval Kinna volcanic succession of Dalslåen et al. (2020) and are interpreted to represent fractionation products of mafic melts derived from metasomatized, highly enriched mantle domains. The tectonic mechanisms responsible for sedimentation and volcanism are not fully resolved, but we envisage two possible explanations: (1) extension and basin subsidence caused by slab retreat and/or breakoff following arc–continent collision and ophiolite obduction, or (2) far-field tectonic forces within the shrinking Iapetan realm. The Trollhøtta–Kinna basin represents a tectonic phase that is apparently not found elsewhere along the Caledonian orogen; volcanic rocks of similar age in southern Norway, Ireland and Newfoundland do not contain the peculiar association of MORB basalts and extremely enriched mafic to felsic rocks which is characteristic for the Trollhøtta–Kinna

basin. The closest analogues are the Lloyds River ophiolite complex of Newfoundland, which is intruded by the shoshonitic Portage Lake monzograbbro.

Acknowledgements

E. W. Stokke assisted in the field and lab, G. Fjeld Bye (UiO) prepared TIMS samples, and the staff at the NGU laboratories provided whole-rock XRF and LA-ICP-MS analyses. Discussions with M. Kristoffersen and T. Andersen are highly appreciated. Constructive feedback from Greg Dunning and Rob Strachan helped to improve the manuscript. This paper is part of the PhD work of B. H. Dalslåen which is funded by the University of Oslo; field work and analyses are partly funded by the Geological Survey of Norway project number 353000.

References

Andersen, T. 2013. Age, Hf isotope and trace element signatures of detrital zircons in the Mesoproterozoic Eriksfjord sandstone, southern Greenland: are detrital zircons reliable guides to sedimentary provenance and timing of deposition? *Geological Magazine*, **150**, 426-440.

Andersen, T., Kristoffersen, M. & Elburg, M.A. 2018. Visualizing, interpreting and comparing detrital zircon age and Hf isotope data in basin analysis–a graphical approach. *Basin Research*, **30**, 132-147.

Andersen, T., Andersson, U.B., Graham, S., Åberg, G. & Simonsen, S.L. 2009. Granitic magmatism by melting of juvenile continental crust: new constraints on the source of Palaeoproterozoic granitoids in Fennoscandia from Hf isotopes in zircon. *Journal of the Geological Society*, **166**, 233-247.

Augland, L.E., Andresen, A. & Corfu, F. 2010. Age, structural setting, and exhumation of the Liverpool Land eclogite terrane, East Greenland Caledonides. *Lithosphere*, **2**, 267-286.

Augland, L.E., Andresen, A., Gasser, D. & Steltenpohl, M.G. 2014. Early Ordovician to Silurian evolution of exotic terranes in the Scandinavian Caledonides of the Ofoten–Troms area–terrane characterization and correlation based on new U–Pb zircon ages and Lu–Hf isotopic data. *In*: Corfu, F., Gasser, D. & Chew, D. (eds) *New Perspectives on the Caledonides of Scandinavia and Related Areas*. Geological Society, London, Special Publications, **390**, 655-678.

Ballo, E.G., Augland, L.E., Hammer, Ø. & Svensen, H.H. 2019. A new age model for the Ordovician (Sandbian) K-bentonites in Oslo, Norway. *Palaeogeography, Palaeoclimatology, Palaeoecology*, **520**, 203-213.

Bingen, B., Demaiffe, D. & Breemen, O.V. 1998. The 616 Ma old Egersund basaltic dike swarm, SW Norway, and late Neoproterozoic opening of the Iapetus Ocean. *The Journal of Geology*, **106**, 565-574.

Bowring, J.F., McLean, N.M. & Bowring, S. 2011. Engineering cyber infrastructure for U-Pb geochronology: Tripoli and U-Pb_Redux. *Geochemistry, Geophysics, Geosystems*, **12**.

Bruton, D.L. & Bockelie, J.F. 1980. Geology and paleontology of the Hølonda area, western Norway—A fragment of North America. *The Caledonides in the USA. Virginia Polytechnic Institute and State University, Department of Geological Sciences Memoir*, **2**, 41-47.

Cawood, P.A., McCausland, P.J. & Dunning, G.R. 2001. Opening Iapetus: constraints from the Laurentian margin in Newfoundland. *Geological Society of America Bulletin*, **113**, 443-453.

Chew, D.M. & Strachan, R.A. 2014. The Laurentian Caledonides of Scotland and Ireland. *In*: Corfu, F., Gasser, D. & Chew, D. (eds) *New Perspectives on the Caledonides of Scandinavia and Related Areas*. Geological Society, London, Special Publications, **390**, 45-91.

Chew, D.M., Graham, J.R. & Whitehouse, M.J. 2007. U–Pb zircon geochronology of plagiogranites from the Lough Nafooey (= Midland Valley) arc in western Ireland: constraints on the onset of the Grampian orogeny. *Journal of the Geological Society*, **164**, 747-750.

Chew, D.M., Daly, J.S., Magna, T., Page, L.M., Kirkland, C.L., Whitehouse, M.J. & Lam, R. 2010. Timing of ophiolite obduction in the Grampian orogen. *Bulletin*, **122**, 1787-1799.

Clift, P. & Ryan, P. 1994. Geochemical evolution of an Ordovician island arc, South Mayo, Ireland. *Journal of the Geological Society*, **151**, 329-342.

Cocks, L.R.M. & Torsvik, T.H. 2011. The Palaeozoic geography of Laurentia and western Laurussia: a stable craton with mobile margins. *Earth-Science Reviews*, **106**, 1-51.

Cooper, M., Crowley, Q. & Rushton, A. 2008. New age constraints for the Ordovician Tyrone Volcanic Group, Northern Ireland. *Journal of the Geological Society*, **165**, 333-339.

Cooper, M., Crowley, Q., Hollis, S., Noble, S., Roberts, S., Chew, D., Earls, G., Herrington, R.*, et al.* 2011. Age constraints and geochemistry of the Ordovician Tyrone Igneous Complex, Northern Ireland: implications for the Grampian orogeny. *Journal of the Geological Society*, **168**, 837-850.

Corfu, F., Andersen, T. & Gasser, D. 2014. The Scandinavian Caledonides: main features, conceptual advances and critical questions. *In*: Corfu, F., Gasser, D. & Chew, D. (eds) *New Perspectives on the Caledonides of Scandinavia and Related Areas*. Geological Society, London, Special Publications, **390**, 9-43.

Crowley, J., Schoene, B. & Bowring, S. 2007. U-Pb dating of zircon in the Bishop Tuff at the millennial scale. *Geology*, **35**, 1123-1126.

Dalslåen, B.H., Gasser, D., Grenne, T., Augland, L.E. & Corfu, F. 2020. Ordovician shoshonitic to ultrapotassic volcanism in the central Norwegian Caledonides: The result of sediment subduction, mantle metasomatism and mantle partial melting. *Lithos*, **356-357**, 105372, http://doi.org/10.1016/j.lithos.2020.105372.

Dickinson, W.R. & Gehrels, G.E. 2009. Use of U–Pb ages of detrital zircons to infer maximum depositional ages of strata: a test against a Colorado Plateau Mesozoic database. *Earth and Planetary Science Letters*, **288**, 115-125.

Domeier, M. 2016. A plate tectonic scenario for the Iapetus and Rheic oceans. *Gondwana Research*, **36**, 275-295.

Draut, A.E., Clift, P.D., Amato, J.M., Blusztajn, J. & Schouten, H. 2009. Arc–continent collision and the formation of continental crust: a new geochemical and isotopic record from the Ordovician Tyrone Igneous Complex, Ireland. *Journal of the Geological Society*, **166**, 485-500.

Dunk, M., Strachan, R., Cutts, K., Lasalle, S., Storey, C., Burns, I., Whitehouse, M.J., Fowler, M.*, et al.* 2019. Evidence for a late Cambrian juvenile arc and a buried suture within the Laurentian Caledonides of Scotland: Comparisons with hyperextended Iapetan margins in the Appalachian Mountains (North America) and Norway. *Geology*, **47**, 734-738.

Dunk, R., Mills, R. & Jenkins, W.J.C.G. 2002. A reevaluation of the oceanic uranium budget for the Holocene. **190**, 45-67.

Dunning, G. & Krogh, T. 1985. Geochronology of ophiolites of the Newfoundland Appalachians. *Canadian Journal of Earth Sciences*, **22**, 1659-1670.

Dunning, G. & Pedersen, R. 1988. U/Pb ages of ophiolites and arc-related plutons of the Norwegian Caledonides: implications for the development of Iapetus. *Contributions to Mineralogy and Petrology*, **98**, 13-23.

Foley, S. 1992. Vein-plus-wall-rock melting mechanisms in the lithosphere and the origin of potassic alkaline magmas. *Lithos*, **28**, 435-453.

Furnes, H. 1985. Geological and geochemical classification of the ophiolitic fragments in the Scandinavian Caledonides. *In*: Gee, D.G. & Sturt, B.A. (eds) *The Caledonide Orogen - Scandinavia and Related Areas*. John Wiley & Sons, Chichester, **2**, 657-669.

Furnes, H., Dilek, Y. & Pedersen, R.B. 2012. Structure, geochemistry, and tectonic evolution of trench-distal backarc oceanic crust in the western Norwegian Caledonides, Solund-Stavfjord ophiolite (Norway). *Bulletin*, **124**, 1027-1047.

Förster, M.W., Prelević, D., Schmück, H.R., Buhre, S., Veter, M., Mertz-Kraus, R., Foley, S.F. & Jacob, D.E. 2017. Melting and dynamic metasomatism of mixed harzburgite+ glimmerite mantle source: Implications for the genesis of orogenic potassic magmas. *Chemical Geology*, **455**, 182-191.

Gale, A., Dalton, C.A., Langmuir, C.H., Su, Y. & Schilling, J.G. 2013. The mean composition of ocean ridge basalts. *Geochemistry, Geophysics, Geosystems*, **14**, 489-518.

Gee, D., Guezou, J., Roberts, D. & Wolff, F. 1985. The central-southern part of the Scandinavian Caledonides. *In*: Gee, D.G. & Sturt, B.A. (eds) *The Caledonide Orogen - Scandinavia and Related Areas*. John Wiley & Sons, Chichester, **1**, 109-133.

Gee, D.G., Janák, M., Majka, J., Robinson, P. & van Roermund, H. 2013. Subduction along and within the Baltoscandian margin during closing of the Iapetus Ocean and Baltica-Laurentia collision. *Lithosphere*, **5**, 169-178.

Grenne, T. & Lagerblad, B. 1985. The Fundsjø Group, central Norway—a Lower Paleozoic island arc sequence: geochemistry and regional implications. *In*: Gee, D.G. & Sturt, B.A. (eds) *The Caledonide orogen-Scandinavia and related areas*. John Wiley & Sons, Chichester, **2**, 745-760.

Grenne, T. & Roberts, D. 1998. The Hølonda Porphyrites, Norwegian Caledonides: geochemistry and tectonic setting of Early–Mid-Ordovician shoshonitic volcanism. *Journal of the Geological Society*, **155**, 131-142.

Grenne, T. & Gasser, D. 2017. The Støren Group greenstones and their relationship to the ophiolite fragments of the western Trondheim Nappe Complex, central Norwegian Caledonides. *EGU General Assembly Conference Abstracts*, 4901.

Harland, W. & Gayer, R. 1972. The Arctic Caledonides and earlier oceans. *Geological Magazine*, **109**, 289-314.

Harper, D., Mac Niocaill, C. & Williams, S. 1996. The palaeogeography of early Ordovician Iapetus terranes: an integration of faunal and palaeomagnetic constraints. *Palaeogeography, Palaeoclimatology, Palaeoecology*, **121**, 297-312.

Hartz, E.H. & Torsvik, T.H. 2002. Baltica upside down: a new plate tectonic model for Rodinia and the Iapetus Ocean. *Geology*, **30**, 255-258.

Hollis, S., Cooper, M., Roberts, S., Earls, G., Herrington, R., Condon, D. & Daly, J. 2013. Evolution of the Tyrone ophiolite, Northern Ireland, during the Grampian–Taconic orogeny: a correlative of the Annieopsquotch Ophiolite Belt of central Newfoundland? *Journal of the Geological Society*, **170**, 861-876.

Hollis, S.P., Roberts, S., Cooper, M.R., Earls, G., Herrington, R., Condon, D.J., Cooper, M.J., Archibald, S.M.*, et al.* 2012. Episodic arc-ophiolite emplacement and the growth of continental margins: Late accretion in the Northern Irish sector of the Grampian-Taconic orogeny. *Bulletin*, **124**, 1702-1723.

Hölttä, P., Balagansky, V., Garde, A.A., Mertanen, S., Peltonen, P., Slabunov, A., Sorjonen-Ward, P. & Whitehouse, M. 2008. Archean of greenland and fennoscandia. *Episodes*, **31**, 13-19.

Jaffey, A., Flynn, K., Glendenin, L., Bentley, W.t. & Essling, A. 1971. Precision measurement of half-lives and specific activities of U 235 and U 238. *Physical Review C*, **4**, 1889.

Kjøll, H.J., Andersen, T.B., Corfu, F., Labrousse, L., Tegner, C., Abdelmalak, M.M. & Planke, S. 2019. Timing of Breakup and Thermal Evolution of a Pre-Caledonian Neoproterozoic Exhumed Magma-Rich Rifted Margin. *Tectonics*, **38**, 1843-1862.

Krogh, T. 1973. A low-contamination method for hydrothermal decomposition of zircon and extraction of U and Pb for isotopic age determinations. *Geochimica et Cosmochimica Acta*, **37**, 485-494.

Levashova, N.M., Bazhenov, M.L., Meert, J.G., Danukalov, K.N., Golovanova, I.V., Kuznetsov, N.B. & Fedorova, N.M. 2015. Paleomagnetism of upper Ediacaran clastics from the South Urals: Implications to paleogeography of Baltica and the opening of the Iapetus Ocean. *Gondwana Research*, **28**, 191-208.

Lissenberg, C.J., Zagorevski, A., McNicoll, V.J., van Staal, C.R. & Whalen, J.B. 2005. Assembly of the Annieopsquotch accretionary tract, Newfoundland Appalachians: Age and geodynamic constraints from syn-kinematic intrusions. *The Journal of Geology*, **113**, 553-570.

Ludwig, K.R. 2003. User's manual for isoplot 3.00, a geochronlogical toolkit for microsoft excel. *Berkeley Geochronl. Cent. Spec. Publ.*, **4**, 25-32.

Mac Niocaill, C., Van der Pluijm, B.A. & Van der Voo, R. 1997. Ordovician paleogeography and the evolution of the Iapetus ocean. *Geology*, **25**, 159-162.

Mattinson, J.M. 2005. Zircon U–Pb chemical abrasion ("CA-TIMS") method: combined annealing and multi-step partial dissolution analysis for improved precision and accuracy of zircon ages. *Chemical Geology*, **220**, 47-66.

Murphy, J.B., Keppie, J.D., Nance, R.D. & Dostal, J. 2010. Comparative evolution of the Iapetus and Rheic Oceans: a North America perspective. *Gondwana Research*, **17**, 482-499.

Nance, R.D. & Murphy, J.B. 2019. Supercontinents and the case for Pannotia. *In*: Wilson, R.W., Houseman, G.A., McCaffrey, K.J.W., Doré, A.G. & Buiter, S.J.H. (eds) *Fifty Years of the Wilson Cycle Concept in Plate Tectonics*. Geological Society, London, Special Publications, **470**, 65-86.

Neuman, R.B. 1984. Geology and paleobiology of islands in the Ordovician Iapetus Ocean: Review and implications. *Geological Society of America Bulletin*, **95**, 1188-1201.

Nilsen, O. & Wolff, F.C. 1989. *Røros og Sveg. Berggrunnskart Røros og Sveg M 1:250000*.

Nilsen, O., Sundvoll, B., Roberts, D. & Corfu, F. 2003. U-Pb geochronology and geochemistry of trondhjemites and a norite pluton from the SW Trondheim Region, Central Norwegian Caledonides. *NORGES GEOLOGISKE UNDERSOKELSE*, **441**, 5-16.

Nordås, J., Amaliksen, K., Brekke, H., Suthern, R., Furnes, H., Sturt, B., Robins, B. & Gee, D. 1985. Lithostratigraphy and petrochemistry of Caledonian rocks on Bømlo, SW Norway. *In*: Gee, D.G. & Sturt, B.A. (eds) *The Caledonide Orogen - Scandinavia and Related Areas*. John Wiley & Sons, Chichester, **2**, 679-692.

Pearce, J.A. 1996. A user's guide to basalt discrimination diagrams. *Trace element geochemistry of volcanic rocks: applications for massive sulphide exploration. Geological Association of Canada, Short Course Notes*, **12**, 79-113.

Pearce, J.A. 2008. Geochemical fingerprinting of oceanic basalts with applications to ophiolite classification and the search for Archean oceanic crust. *Lithos*, **100**, 14-48.

Pedersen, R. & Furnes, H. 1991. Geology, magmatic affinity and geotectonic environment of some Caledonian ophiolites in Norway. *Journal of Geodynamics*, **13**, 183-203.

Pedersen, R., Bruton, D. & Furnes, H. 1992. Ordovician faunas, island arcs and ophiolites in the Scandinavian Caledonides. *Terra Nova*, **4**, 217-222.

Pedersen, R.B. & Dunning, G.R. 1997. Evolution of arc crust and relations between contrasting sources: U-Pb (age), Nd and Sr isotope systematics of the ophiolitic terrain of SW Norway. *Contributions to Mineralogy and Petrology*, **128**, 1-15.

Pisarevsky, S.A., Murphy, J.B., Cawood, P.A. & Collins, A.S. 2008. Late Neoproterozoic and Early Cambrian palaeogeography: models and problems. *In*: Pankhurst, R.J., Trouw, R.A.J., de Brito Neves, B.B. & de Wit, M.J. (eds) *West Gondwana: Pre-Cenozoic Correlations Across the South Atlantic Region*. Geological Society, London, Special Publications, **294**, 9-31.

Roberts, D., Nordgulen, O. & Melezhik, V. 2007. The Uppermost Allochthon in the Scandinavian Caledonides: From a Laurentian ancestry through Taconian orogeny to Scandian crustal growth on Baltica. *In*: Hatcher, R.D.J., Carlson, M.P., McBride, J.H. & Martínez Catalán, J.R. (eds) *4-D Framework of Continental Crust*. Geological Society of America Memoir, Boulder, Colorado, **200**, 357-377.

Rohr-Torp, E. 1972. A major inversion of the western part of the Trondheim nappe. *Norsk Geologisk Tidsskrift*, **52**, 453-458.

Ryan, P., Floyd, P. & Archer, J. 1980. The stratigraphy and petrochemistry of the Lough Nafooey Group (Tremadocian), western Ireland. *Journal of the Geological Society*, **137**, 443-458.

Schmitz, M.D. & Schoene, B. 2007. Derivation of isotope ratios, errors, and error correlations for U-Pb geochronology using 205Pb-235U-(233U)-spiked isotope dilution thermal ionization mass spectrometric data. *Geochemistry, Geophysics, Geosystems*, **8**.

Selbekk, R.S., Furnes, H., Pedersen, R.-B. & Skjerlie, K.P. 1998. Contrasting tonalite genesis in the Lyngen magmatic complex, north Norwegian Caledonides. *Lithos*, **42**, 243-268.

Sircombe, K.N. & Stern, R.A. 2002. An investigation of artificial biasing in detrital zircon U-Pb geochronology due to magnetic separation in sample preparation. *Geochimica et Cosmochimica Acta*, **66**, 2379-2397.

Slagstad, T. & Kirkland, C.L. 2017. The use of detrital zircon data in terrane analysis: A nonunique answer to provenance and tectonostratigraphic position in the Scandinavian Caledonides. *Lithosphere*, **9**, 1002-1011.

Slagstad, T. & Kirkland, C.L. 2018. Timing of collision initiation and location of the Scandian orogenic suture in the Scandinavian Caledonides. *Terra Nova*, **30**, 179-188.

Slagstad, T., Davidsen, B. & Daly, J.S. 2011. Age and composition of crystalline basement rocks on the Norwegian continental margin: offshore extension and continuity of the Caledonian–Appalachian orogenic belt. *Journal of the Geological Society*, **168**, 1167-1185.

Slagstad, T., Pin, C., Roberts, D., Kirkland, C.L., Grenne, T., Dunning, G., Sauer, S. & Andersen, T. 2014. Tectonomagmatic evolution of the Early Ordovician suprasubduction-zone ophiolites of the Trondheim Region, Mid-Norwegian Caledonides. *In*: Corfu, F., Gasser, D. & Chew, D. (eds) *New*

Perspectives on the Caledonides of Scandinavia and Related Areas. Geological Society, London, Special Publications, **390**, 541-561.

Slagstad, T., Saalmann, K., Kirkland, C.L., Høyen, A.B., Storruste, B.K., Coint, N., Pin, C., Marker, M.*, et al.* 2020. Late Neoproterozoic through Silurian tectonic evolution of the Rödingsfjället Nappe Complex, orogen-scale correlations and implications for the Scandian suture. *In*: Murphy, J.B., Strachan, R. & Quesada, C. (eds) *Pannotia To Pangaea: Neoproterozoic and Paleozoic Orogenic Cycles in the Circum-Atlantic Region*. Geological Society, London, Special Publications, **503**, SP503-2020-2010.

Spandler, C. & Pirard, C. 2013. Element recycling from subducting slabs to arc crust: A review. *Lithos*, **170**, 208-223.

Stokke, E.W., Gasser, D., Dalslåen, B.H. & Grenne, T. 2018. Tectonic evolution of syn-to late-orogenic sedimentary–volcanic basins in the central Norwegian Caledonides. *Journal of the Geological Society*, **175**, 605-618.

Strachan, R., Prave, A., Kirkland, C. & Storey, C. 2013. U–Pb detrital zircon geochronology of the Dalradian Supergroup, Shetland Islands, Scotland: implications for regional correlations and Neoproterozoic–Palaeozoic basin development. *Journal of the Geological Society*, **170**, 905-916.

Sturt, B., Furnes, H. & Roberts, D. 1984. A conspectus of Scandinavian Caledonian ophiolites. *In*: Gass, I.G., Lippard, S.J. & Shelton, A.W. (eds) *Ophiolites and Oceanic Lithosphere*. Geological Society, London, Special Publications, **13**, 381-391.

Sun, S.-S. & McDonough, W.-s. 1989. Chemical and isotopic systematics of oceanic basalts: implications for mantle composition and processes. *Geological Society, London, Special Publications*, **42**, 313-345.

Swinden, H.S., Jenner, G.A., Szybinski, Z.A., Sinha, A.K., Whalen, J.B. & Hogan, J.P. 1997. Magmatic and tectonic evolution of the Cambrian-Ordovician Laurentian margin of Iapetus: Geochemical and isotopic constraints from the Notre Dame Subzone, Newfoundland. *In*: Krishna Sinha, A., Whalen, J.B. & Hogan, J.P. (eds) *The nature of magmatism in the Appalachian orogen*. Geological Society of America Memoir, Boulder, Colorado, **191**, 337-365.

Tegner, C., Andersen, T.B., Kjøll, H.J., Brown, E.L., Hagen-Peter, G., Corfu, F., Planke, S. & Torsvik, T.H. 2019. A mantle plume origin for the Scandinavian Dyke Complex: a "piercing point" for 615 Ma plate reconstruction of Baltica? *Geochemistry, Geophysics, Geosystems*, **20**, 1075-1094.

Torsvik, T. & Cocks, L. 2016. *Earth History and Palaeogeography.* Cambridge University Press., Cambridge.

Van Staal, C., Whalen, J., McNicoll, V., Pehrsson, S., Lissenberg, C.J., Zagorevski, A., Van Breemen, O. & Jenner, G. 2007. The Notre Dame arc and the Taconic orogeny in Newfoundland. *Geological Society of America Memoirs*, **200**, 511-552.

van Staal, C., Chew, D., Zagorevski, A., McNicoll, V., Hibbard, J., Skulski, T., Castonguay, S., Escayola, M.*, et al.* 2013. Evidence of Late Ediacaran Hyperextension of the Laurentian Iapetan Margin in the Birchy Complex, Baie Verte Peninsula, Northwest Newfoundland:: Implications for the Opening of Iapetus, Formation of Peri-Laurentian Microcontinents and Taconic–Grampian Orogenesis. *Geoscience Canada*, **40**, 94-117.

van Staal, C.R., Whalen, J.B., Valverde-Vaquero, P., Zagorevski, A. & Rogers, N. 2009. Pre-Carboniferous, episodic accretion-related, orogenesis along the Laurentian margin of the northern Appalachians. *Geological Society, London, Special Publications*, **327**, 271-316.

Viken, A.L. 2017. *Accretionary history of Lower Ordovician island arc complexes on Bømlo: evidence from detrital zircon dating and geochemical data.* Master, University of Bergen.

Vogt, T. 1945. The geology of part of the Hølonda-Horg district, a type area in the Trondheim region. *Norsk Geologisk Tidsskrift*, **25**, 449-528.

Waldron, J.W., Schofield, D.I., Murphy, J.B. & Thomas, C.W. 2014. How was the Iapetus Ocean infected with subduction? *Geology*, **42**, 1095-1098.

Wilson, J.T. 1966. Did the Atlantic close and then re-open? *Nature*, **211**, 676-681.

Wolff, F. 1979. Beskrivelse til de berggrunnsgeologiske kart Trondheim og Østersund 1:250 000. *NGU Skrifter*, **353**, 1-76.

Yoshinobu, A.S., Barnes, C.G., Nordgulen, Ø., Prestvik, T., Fanning, M. & Pedersen, R. 2002. Ordovician magmatism, deformation, and exhumation in the Caledonides of central Norway: An orphan of the Taconic orogeny? *Geology*, **30**, 883-886.

Zagorevski, A. & Van Staal, C. 2011. The record of Ordovician arc–arc and arc–continent collisions in the Canadian Appalachians during the closure of Iapetus. *In*: Brown, D. & Ryan, P. (eds) *Arc-continent collision*. Springer, Berlin, 341-371.

Zagorevski, A., Van Staal, C.R., Rogers, N., McNicoll, V.J. & Pollock, J. 2010. Middle Cambrian to Ordovician arc-backarc development on the leading edge of Ganderia, Newfoundland Appalachians. *Memoir of the Geological Society of America*, **206**, 367-396, http://doi.org/10.1130/2010.1206(16).

Zagorevski, A., Rogers, N., Van Staal, C., McNicoll, V., Lissenberg, C.J. & Valverde-Vaquero, P. 2006. Lower to Middle Ordovician evolution of peri-Laurentian arc and backarc complexes in Iapetus: Constraints from the Annieopsquotch accretionary tract, central Newfoundland. *Geological Society of America Bulletin*, **118**, 324-342.

Figure captions

Fig. 1: (**a**) 420 Ma tectonic reconstruction (Cocks & Torsvik 2011) with the main units of the Caledonian orogen after Hollis et al. (2012). (**b**) Map of the Scandinavian Caledonides, with localities mentioned in the text, LVB = Løkken–Vassfjellet–Bymarka ophiolite. (**c**) overview map of the British–Irish Caledonides with localities mentioned in the text, after Hollis et al. (2012). (**d**) Overview map of Newfoundland with localities mentioned in the text, after Hollis et al. (2012).

Fig. 2: Geological map of the Oppdal area with sample localities; the symbols for the geochemistry samples correspond to those of figures 6 and 7.

Fig. 3: Interpretative geological profiles; section A-B is from the Dugurdskmappen–Gisnadalen section, with comparison to the interpretation of Rohr-Torp (1972). The insert profile in section A-B is from Stokke et al. (2018). Section C-D is from the the Vinstradalen fault trough the Skarvatnet unit to the Oppdal area.

Fig. 4: Field photos from the Gisnadalen section. (**a**) Graded bed at the bottom of the Gisnadalen section [UTM(32)543369.6955781]. (**b**) Coarse-grained sandstone from Gisnadalen. Locality of

detrital zircon sample 15BD_186 [UTM(32)543291.6956043]. (**c**) Polymict conglomerate with felsic volcanic and siltstone clasts [UTM(32)539046.6957637]. (**d**) Silty grey chert with thin siltstone beds [UTM(32)538461.6959290]. (**e**) Alkali rhyolite with a fragmental texture. Picture is from the volcanic deposit dated at 473±1 Ma, taken 300 m NNE of the sampling locality [UTM (32)538138.6958005]. (**f**) Inverted pillow lava [UTM (32)535360.6953739]. (**g**) Close-up of bedded jasper. Picture is from Vangslia area [UTM (32)537433.6958089]. (**h**) Black, magnetic chert, magnet is 2 cm [UTM (32)536832.6957001].

Fig. 5: Field photos from the Oppdal–Skjørstadhovden–Stølen area. (**a**) Grey chert with siltstone layers, Skjørstadhovden [UTM (32)535428.6942809]. (**b**) Well preserved, overturned pillow lava with internal tabular shelves, Stølen [UTM (32)538140.6943500]. (**c**) Fine-grained sandstone where grading suggests overturned bedding; west of Skjørstadhovden [UTM (32)532073.6943731]. (**d**) Granule conglomerate, Oppdal city centre. Clasts consist of greenstone, jasper, biotite aggregates, felsic volcanic rock fragments, and quartz [UTM (32)534174.6940606].

Fig. 6: Geochemistry plots. (**a**) TAS plot. (**b**) Classification based on the stable elements Zr, Ti, Nb and Y (Pearce 1996). (**c**) Th/Yb vs. Nb/Yb plot (Pearce 2008) with fields of volcanic rocks from oceanic and continental arcs. All felsic samples from the Trollhøtta basin are highly enriched compared to normal arc rocks, while basaltic samples fall in the oceanic range.

Fig. 7: Multi element plots. Left column: MORB-normalized patterns; normalising values are from average N-MORB data of Gale et al. (2013). Right column: Chondrite normalized patterns; chondrite values from Sun & McDonough (1989). In Fig. 7e and f, the patterns of the Kinna volcanic succession and the Storgruvpiken rhyolite from Dalslåen et al. (2020) are added (grey and stippled) for comparison with the felsic Trollhøtta rocks.

Fig. 8: Concordia plots for the zircon U-Pb TIMS data. Data point ellipses are 2σ; plots are made with ISOPLOT (Ludwig 2003). (**a**) Sample 1: alkali rhyolite with a mean age of 472.4 ± 0.7 Ma (2σ; MSWD = 0.22). (**b**) Sample 2: alkali rhyolite bed with a mean age of 473.3 ± 1.0 Ma (2σ; MSWD = 0.87).

Fig. 9: Detrital zircon plots of U-Pb ages; combined histograms and kernel density estimates (KDE). All detrital zircon U-Pb age plots are made with the detzrcr software package for R (Andersen et al. 2018). Band width = 25. All data shown are less than 10% discordant, the Caledonian populations are shown separately and represent data less than 5% discordant.

Fig. 10: (**a**) Plot of the cumulative distribution of zircon U-Pb ages (Andersen et al. 2018). (**b**) Upper/lower quartile plot of zircon U/Pb ages (Andersen et al. 2018).

Table 1: Major and trace element analyses. Elements in italics are analysed on ICP-MS, other elements are analysed on XRF.

Table 2: ID-TIMS U-Pb zircon analytical data.

Table 1

Group	N-MORB																
Sample	TGR_198	TGR_206 A	TGR_206 B	TGR_208	TGR_209	TGR_213 A	14BD_73	BD15_1266	15BD_64	15BD_183	15BD_183B	15BD_191	15BD_811	15BD_865	15BD_1001	15BD_1331	15BD_1551	15BD_1606
UTM(32)	537915.6943470	5381469435 00	5381469435 00	537575.6943535	538175.6943837	535502.6943122	535360.6953739	5327788.6943561	532047.6939412	5433711.6955849	5433711.6955849	5431506.6956479	5367403.6955706	5387706.6957103	536201.6959370	537025.6957995	534817.6956841	537790.6957673
SiO_2 %	46.3	47.5	46.5	47.3	46.5	46.6	48.0	50.2	43.5	50.3	48.0	48.2	49.4	46.9	52.7	48.5	47.7	49.0
Al_2O_3	14.9	15.5	15.4	15.8	14.0	15.7	12.6	18.4	10.2	18.3	15.3	15.3	15.3	15.1	17.8	13.0	14.7	15.8
Fe_2O_3	10.4	12.5	12.0	12.6	13.1	11.0	8.65	12.2	12.0	12.4	11.1	11.1	9.49	10.6	12.4	8.99	9.92	8.89
TiO_2	1.68	1.78	1.86	1.87	2.23	1.91	1.44	1.94	1.64	2.28	2.10	2.14	1.96	1.71	2.17	1.47	1.76	1.55
MgO	7.85	6.18	6.20	6.24	6.55	6.33	4.81	2.12	12.3	2.40	9.61	5.21	5.75	7.54	2.01	9.17	7.16	7.71
CaO	9.47	9.86	10.8	8.72	9.35	10.0	10.8	3.48	10.2	2.92	5.26	11.0	10.6	10.1	2.33	12.7	9.97	9.66
Na_2O	2.93	3.15	3.09	3.16	3.49	3.69	3.32	3.29	1.97	3.72	1.93	3.46	3.37	2.52	7.13	2.13	3.55	2.75
K_2O	0.393	0.737	0.238	0.449	0.172	0.402	0.261	4.14	0.094	4.06	0.177	0.111	0.444	0.160	0.856	0.203	0.212	0.148
MnO	0.167	0.160	0.180	0.162	0.205	0.171	0.148	0.245	0.181	0.118	0.174	0.183	0.140	0.147	0.104	0.140	0.140	0.153
P_2O_5	0.179	0.170	0.172	0.175	0.245	0.177	0.172	0.349	0.219	0.295	0.251	0.248	0.230	0.192	0.329	0.125	0.203	0.181
LOI	5.00	1.91	2.47	2.45	3.60	3.01	8.53	2.93	6.37	2.04	5.34	1.86	2.02	3.66	1.33	2.59	3.22	3.50
Ba (ppm)	<10	<10	<10	<10	<10	<10	37	630	<10	363	17	28	76	22	157	51	45	39
Co	43.8	45.9	44.8	50.6	49.2	47.7	32.1	26.1	71.9	36.1	42.2	33.9	24.7	40.6	51.5	41.2	45.1	39.3
Cr	287	273	284	296	116	286	359	525	930	270	332	264	274	331	277	688	448	358
Cu	49.5	38.5	44.0	37.8	55.5	51.0	49.0	61.5	36.6	92.8	<5	32.0	140	42.6	<5	47.7	44.8	50.9
Ga	15.8	16.0	17.1	16.2	18.1	17.9	12.7	19.1	12.1	20.9	16.9	17.5	17.6	16.4	12.9	16.2	16.3	16.6
Ni	75.5	105	111	126	53.5	124	145	104	498	96.5	132	106	106	153	168	309	197	138
Pb	5.7	<5	<5	<5	<5	<5	<5	12.5	<5	5.1	5.7	<5	<5	<5	<5	<5	<5	5.4
Rb	<5	17.0	<5	11.1	<5	5.4	6.9	89.7	<5	82.7	<5	<5	8.7	<5	16.5	<5	<5	<5
Sc	32.3	31.5	34.7	35.6	40.4	30.5	29.1	42.0	27.3	31.1	27.3	27.9	29.1	25.8	18.9	27.4	26.8	28.4
Sn	<5	<5	<5	<5	<5	<5	<5	<5	<5	<5	<5	<5	<5	<5	<5	<5	<5	<5
Sr	224	188	167	181	121	206	285	234	50.5	218	250	328	346	259	108	334	108	192
V	312	339	332	321	393	332	286	132	255	48.2	294	327	346	265	104	272	284	279

Y	29.9	33.0	35.8	33.5	49.4	36.6	29.6	44.6	21.8	46.1	41.3	35.7	31.6	31.6	28.5	29.2	24.2	23.9
Zn	78.6	89.4	85.1	96.0	113	91.1	53.8	80.2	85.5	86.5	96.3	74.4	56.6	74.3	94.0	46.4	67.8	64.1
Zr	118	109	116	114	162	118	115	145	101	185	180	151	132	117	161	99.2	104	93
Cs	<10	<10	<10	<10	<10	<10	<10	5.48	<0.4	5.33	0.82	<0.4	0.80	0.61	0.61	0.52	<0.4	<0.4
Ge	N.A	N.A	N.A	N.A	N.A	N.A	N.A	<2	N.A	N.A	N.A	N.A	N.A	N.A	N.A	N.A	N.A	N.A
Be	<1	1.1	1.1	<1	1.3	1.0	<1	<1	<1	1.3	<1	<1	<1	<1	<1	<1	<1	<1
Nb	7.30	6.62	7.14	5.75	7.27	6.96	6.20	7.51	5.92	13.1	12.2	8.03	6.58	4.77	8.30	5.05	4.23	7.54
La	8.17	7.64	6.99	6.81	8.53	7.10	7.45	9.64	7.30	15.7	11.6	10.6	7.44	6.29	11.6	6.06	5.84	6.83
Ce	20.2	18.8	17.8	16.3	21.8	18.8	18.9	24.7	20.0	38.2	28.2	28.5	21.0	17.0	27.1	15.4	16.5	17.1
Pr	2.89	2.66	2.64	2.54	3.19	2.67	2.72	3.94	2.88	5.84	4.19	4.01	3.20	2.70	3.93	2.42	2.50	2.45
Nd	14.4	14.0	14.0	14.1	18.2	14.1	14.6	20.2	13.3	28.8	20.8	19.7	15.8	13.9	18.8	12.1	12.4	11.6
Sm	4.35	4.27	4.44	4.47	5.98	4.88	4.56	6.59	4.13	8.67	6.53	6.14	5.22	4.38	5.56	3.96	4.12	3.68
Eu	1.69	1.67	1.73	1.55	1.97	1.74	1.52	2.39	1.18	2.97	1.94	2.29	1.93	1.78	1.79	1.86	1.57	1.48
Gd	4.84	4.90	5.55	5.00	7.06	5.23	4.81	7.53	4.14	9.15	6.97	6.34	5.95	5.05	6.24	4.74	4.51	4.15
Tb	0.97 0	1.20	1.12	1.05	1.41	1.03	0.91 0	1.40	0.75 5	1.58	1.24	1.15	1.05	0.910	1.03	0.866	0.846	0.781
Dy	5.62	5.79	6.26	6.14	8.79	6.43	5.67	8.90	4.77	9.80	7.94	7.27	6.61	5.69	6.09	5.54	5.13	4.80
Ho	1.24	1.24	1.37	1.33	1.93	1.42	1.21	1.90	0.96 9	2.01	1.70	1.48	1.41	1.20	1.24	1.21	1.08	1.03
Er	3.29	3.11	3.86	3.73	5.34	3.87	3.24	4.77	2.48	4.86	4.31	3.73	3.71	3.24	3.05	3.27	2.91	2.82
Tm	0.47 3	0.505	0.545	0.47 5	0.73 7	0.526	0.53 4	0.678	0.35 1	0.675	0.626	0.559	0.547	0.518	0.437	0.517	0.417	0.421
Yb	2.74	2.90	3.53	3.24	4.53	3.50	3.17	4.27	2.11	3.79	3.59	3.49	3.42	3.05	2.59	3.14	2.65	2.60
Lu	0.44 2	0.458	0.515	0.51 2	0.74 6	0.517	0.47 3	0.588	0.26 0	0.531	0.515	0.455	0.509	0.446	0.392	0.481	0.394	0.377
Hf	2.99	2.77	2.90	3.09	4.30	3.12	3.22	3.82	2.70	4.53	4.47	3.80	3.52	2.97	4.03	2.89	2.79	2.48
Ta	0.53 1	0.514	0.519	0.44 3	0.59 0	0.515	0.38 8	0.518	0.46 7	0.875	0.785	0.529	0.423	0.317	0.767	0.371	0.300	0.475
W	N.A	N.A	N.A	N.A	N.A	N.A	N.A	1.12	0.85	0.93	0.85	0.89	0.64	0.46	<0.2	0.47	0.30	0.47
Bi	0.05 1	<0.5	<0.5	<0.5	<0.5	<0.5	<0.5	<0.5	<0.5	<0.5	<0.5	<0.5	<0.5	<0.5	<0.5	<0.5	<0.5	<0.5
Th	0.56 5	0.475	0.573	0.52 6	0.66 0	0.512	0.53 6	0.938	1.05	1.16	1.57	0.613	0.893	0.380	0.933	0.477	0.333	0.582
U	0.19 3	0.182	0.175	0.14 1	0.57 8	0.508	0.26 9	0.742	0.23 6	0.414	0.343	0.288	0.277	0.177	0.216	0.241	0.202	0.234
La_N/L	1.91			1.37	1.18		1.62		2.90									
u_N	1	1.724	1.403	5	2	1.420	8	1.695	2	3.056	2.328	2.408	1.511	1.458	3.059	1.302	1.532	1.873
Sm/L	0.53			0.65	0.70		0.61		0.56									
a	2	0.559	0.635	6	1	0.687	2	0.684	6	0.552	0.563	0.579	0.702	0.696	0.479	0.653	0.705	0.539

Th/La	0.069	0.062	0.082	0.077	0.077	0.072	0.072	0.097	0.144	0.074	0.135	0.058	0.120	0.060	0.080	0.079	0.057	0.085
Mg#	57	47	48	47	47	51	50	24	65	26	61	46	52	56	22	65	56	61

Group	D-MORB						E-MORB			Enriched			
Sample	15BD_209	15BD_658	15BD_44	15BD_816	15BD_1700	15BD_1198	15BD_1513	15BD_1734	14BD_82	15BD_1003	14BD_83	15BD_788	15BD_828
UTM (32)	542407.6957418	533366.6953380	535377.6939519	536816.6955520	539492.6957561	534772.6959798	536288.6958967	537406.6958079	537665.6958234	535994.6959168	531306.6945925	532465.6951299	537057.6955508
SiO_2 (%)	46.5	49.9	47.6	48.0	47.6	48.3	51.9	49.8	51.1	65.5	62.5	69.5	63.1
Al_2O_3	15.7	14.0	13.8	14.9	13.5	13.8	15.0	15.1	14.6	16.3	17.5	14.4	17.2
Fe_2O_3	9.26	6.39	14.0	9.41	13.1	10.1	7.35	10.8	8.46	1.64	3.21	2.02	3.99
TiO_2	0.876	1.09	2.51	1.25	1.95	1.43	1.13	2.29	1.85	0.142	0.313	0.329	0.569
MgO	7.67	6.10	6.82	7.87	6.34	9.49	5.83	6.77	4.74	0.460	1.29	1.36	1.49
CaO	9.33	10.6	7.57	9.77	11.6	10.4	10.3	5.75	9.17	2.36	1.58	1.52	1.73
Na_2O	3.76	5.02	3.79	3.19	2.36	2.59	4.00	4.58	3.01	8.44	7.47	4.81	5.86
K_2O	0.303	0.269	0.205	0.106	0.086	0.078	0.062	0.704	0.583	0.926	2.54	2.76	2.96
MnO	0.136	0.121	0.209	0.147	0.200	0.170	0.109	0.179	0.082	0.143	0.074	0.064	0.068
P_2O_5	0.049	0.077	0.292	0.099	0.172	0.128	0.124	0.399	0.278	0.080	0.153	0.089	0.153
LOI	5.09	5.93	2.29	4.05	1.80	2.35	2.83	2.65	4.14	2.08	2.03	2.42	1.67
Ba (ppm)	24	34	20	<10	<10	13	22	159	87	113	162	412	336
Co	39.5	30.3	40.7	33.8	40.8	38.5	26.4	37.7	46.9	<4	5.1	<4	6.1
Cr	402	258	157	265	132	406	297	192	412	8.9	6.5	16.2	23.4
Cu	96.1	9.6	8.9	89.4	21.2	9.5	43.8	54.1	92.2	80.2	<5	<5	73.4
Ga	12.1	10.3	16.8	14.8	17.1	14.6	12.8	14.7	17.1	14.5	16.2	19.4	25.4
Ni	126	133	65.9	112	56.4	157	117	100	196	<5	10.1	9.4	9.4
Pb	<5	<5	<5	<5	<5	<5	<5	<5	<5	70.4	25.6	21.0	31.8
Rb	<5	6.2	<5	<5	<5	<5	<5	13.7	10.2	26.6	139	129	164
Sc	30.0	26.1	31.3	26.5	33.2	25.6	27.3	27.4	24.0	<5	6.0	<5	5.6
Sn	<5	<5	<5	<5	<5	<5	<5	<5	<5	5.2	7.2	7.3	7.4
Sr	118	124	97.6	185	185	151	252	123	308	322	270	187	304
V	251	190	416	233	390	255	237	290	314	5.8	7.7	10.2	26.9
Y	24.6	19.5	41.7	23.1	36.7	30.2	16.3	39.2	35.0	48.8	32.4	71.2	65.4

Zn	69.3	47.4	120	73.4	88.8	65.7	40.2	104	59.7	51.9	62.8	53.1	89.0
Zr	46.7	60.0	141	67.5	118	102	62.4	214	182	749	1030	727	1020
Cs	<0.4	<0.4	0.77	<0.4	<0.4	<0.4	<0.4	<0.4	<10	19	23	6.52	8.05
Ge	N.A	N.A	N.A	N.A	N.A	N.A	N.A	N.A	N.A	N.A	N.A	<2	<2
Be	<1	<1	<1	<1	<1	<1	<1	1.3	<1	5.3	7.3	7.6	8.8
Nb	0.494	1.46	6.49	1.33	4.03	2.37	7.28	24.4	19.5	23.0	34.9	32.2	49.1
La	1.36	2.07	7.33	2.28	5.75	4.93	6.27	19.9	15.6	411	272	315	199
Ce	4.79	6.90	21.4	7.57	16.1	13.5	14.6	44.2	33.5	624	455	412	330
Pr	0.993	1.22	3.32	1.38	2.66	2.21	1.89	5.93	4.54	65.0	46.1	56.3	40.6
Nd	6.06	7.29	17.3	7.83	14.4	11.8	8.85	26.7	22.4	208	154	199	149
Sm	2.48	2.77	5.97	3.10	5.22	4.09	2.62	7.38	6.21	23.8	18.4	35.4	30.1
Eu	1.10	1.07	1.92	1.26	2.00	1.57	1.06	2.38	2.08	1.15	1.51	3.00	2.71
Gd	3.40	3.35	6.92	3.72	6.11	4.98	2.95	7.85	6.37	12.1	9.28	25.8	21.3
Tb	0.678	0.606	1.30	0.702	1.17	0.882	0.519	1.34	1.14	1.56	1.25	3.67	2.96
Dy	4.85	3.74	8.27	4.53	7.71	5.77	3.26	8.33	7.49	8.41	6.57	17.6	14.7
Ho	1.06	0.834	1.79	0.980	1.64	1.20	0.677	1.76	1.53	1.63	1.22	2.74	2.50
Er	2.78	2.35	4.58	2.75	4.56	3.38	1.93	4.55	3.87	4.57	3.30	5.78	5.83
Tm	0.437	0.333	0.700	0.401	0.689	0.489	0.268	0.657	0.596	0.691	0.534	0.740	0.843
Yb	2.59	2.06	4.35	2.49	4.19	3.01	1.75	4.05	3.62	4.58	3.59	4.10	4.40
Lu	0.324	0.323	0.561	0.369	0.659	0.468	0.261	0.590	0.533	0.828	0.543	0.556	0.601
Hf	1.55	1.69	4.06	1.97	3.29	2.75	1.65	5.24	4.37	20.1	24.4	20.2	26.7
Ta	0.058	0.098	0.409	0.095	0.275	0.168	0.426	1.46	1.13	1.65	1.60	2.04	2.83
W	0.57	0.32	0.64	0.22	0.56	0.20	0.21	0.60	N.A	0.55	N.A	2.97	2.73
Bi	<0.5	<0.5	<0.5	<0.5	<0.5	<0.5	<0.5	<0.5	<0.5	<0.5	<0.5	<0.5	<0.5
Th	0.069	0.209	0.543	0.126	0.323	0.433	0.644	1.98	2.22	105	75.0	67.0	67.9
U	0.022	0.150	0.386	0.090	0.148	0.137	0.248	0.520	0.540	15.0	15.6	12.4	12.7
La_N/Lu_N	0.434	0.662	1.351	0.639	0.902	1.089	2.483	3.487	3.026	51.313	51.783	58.567	34.229
Sm/La	1.824	1.338	0.814	1.360	0.908	0.830	0.418	0.371	0.398	0.058	0.068	0.112	0.151
Th/La	0.051	0.101	0.074	0.055	0.056	0.088	0.103	0.099	0.142	0.255	0.276	0.213	0.341
Mg#	60	63	46	60	46	63	59	53	50	33	42	55	40

Table 2

U-Th-Pb isotopic data

		Compositional Parameters											Isotopic Ages					
Sample	Wt. mg	U ppm	Th/U	Pb*/Pb$_c$	Pb$_c$ (pg)	$^{207}Pb/^{206}Pb$	% err	$^{207}Pb/^{235}U$	% err	$^{206}Pb/^{238}U$	% err	corr. coef.	$^{207}Pb/^{206}Pb$	±	$^{207}Pb/^{235}U$	±	$^{206}Pb/^{238}U$	±
(a)	(b)	(c)	(d)	(e)	(e)	(g)	(h)	(g)	(h)	(g)	(h)		(i)	(h)	(i)	(h)	(i)	(h)
15BD_828																		
1	0.001	34	0.90	2.8	1.1	0.0577	3.3	0.605	3.4	0.076147	0.33	0.351	517	72	479	13	473.1	1.5
2	0.001	22	0.91	1.9	1.0	0.0581	6.1	0.612	6.3	0.076336	0.70	0.359	535	133	485	24	474.2	3.2
3	0.001	30	0.84	2.1	1.2	0.0582	4.6	0.611	4.8	0.076097	0.37	0.501	538	101	484	19	472.8	1.7
4	0.001	26	0.83	1.7	1.3	0.0575	6.0	0.607	6.2	0.076522	0.65	0.362	511	132	482	24	475.3	3.0
14BD_83																		
1	0.006	232	0.81	91	1.3	0.05657	0.23	0.5930	0.36	0.076027	0.24	0.762	472.6	5.2	471.0	1.4	472.4	1.1
2	0.003	131	n.m	43	1.2	0.05583	0.54	0.5819	0.63	0.075586	0.24	0.520	443	12	465.7	2.3	469.7	1.1
3	0.001	1818	n.m	241	0.57	0.05642	0.09	0.5911	0.28	0.07599	0.25	0.990	466.5	2.0	471.6	1.0	472.1	1.1
4	0.006	132	n.m	38	1.4	0.05661	0.45	0.5899	0.60	0.075581	0.36	0.669	474	10	470.8	2.3	469.7	1.6
5	0.001	198	n.m	17	1.5	0.05738	0.88	0.6019	0.96	0.076085	0.27	0.425	504	19	478.4	3.7	472.7	1.2

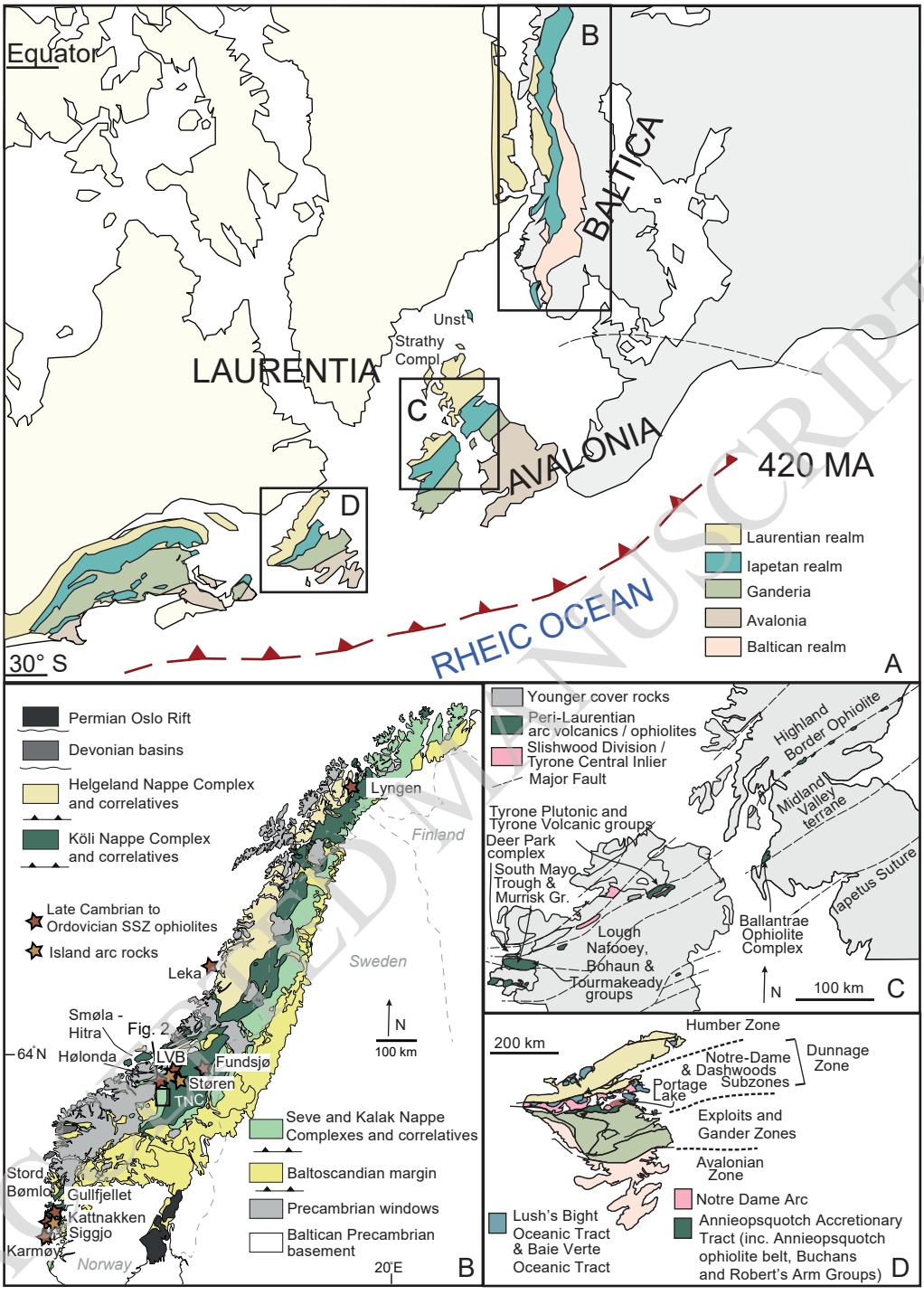

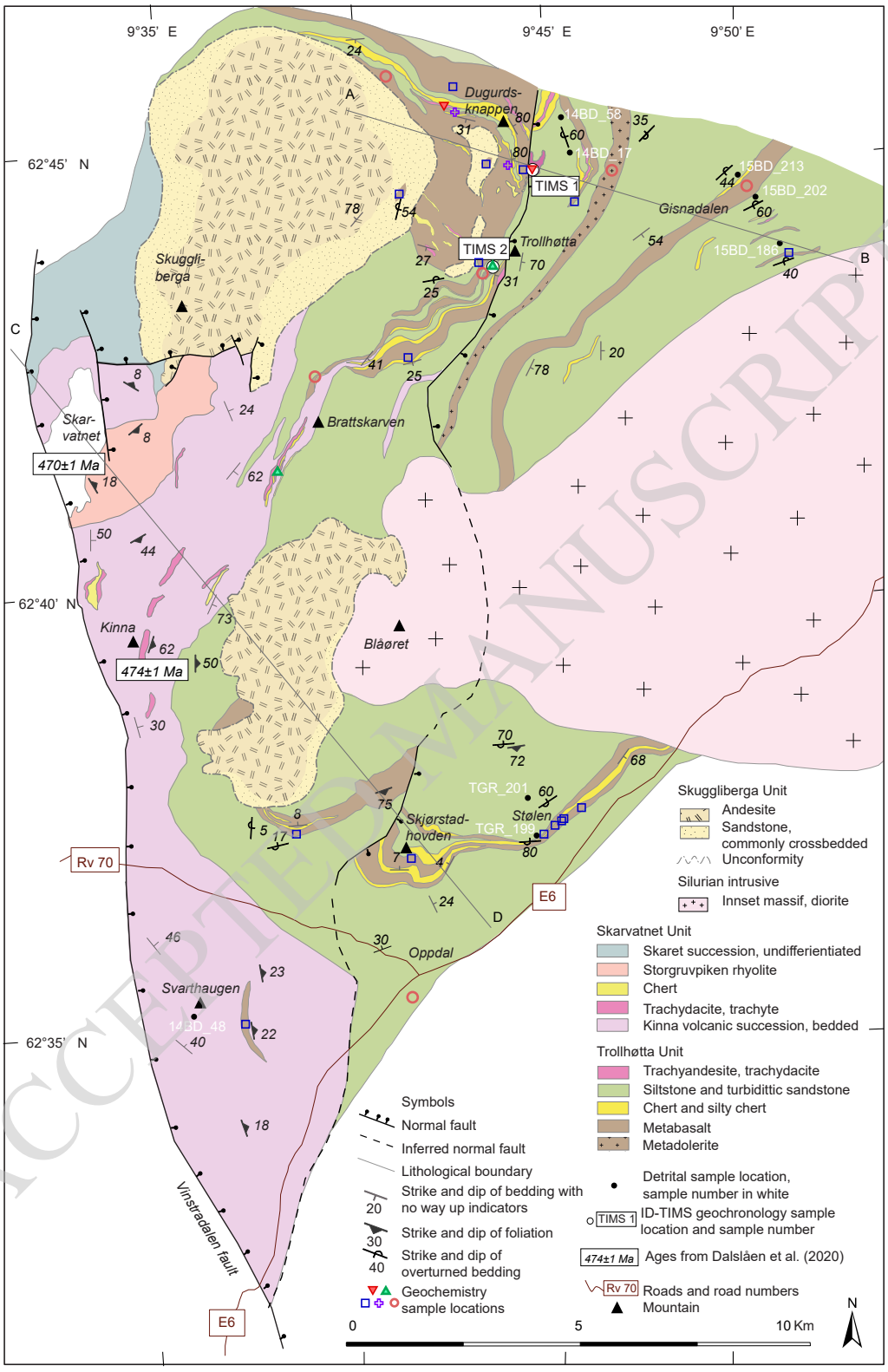

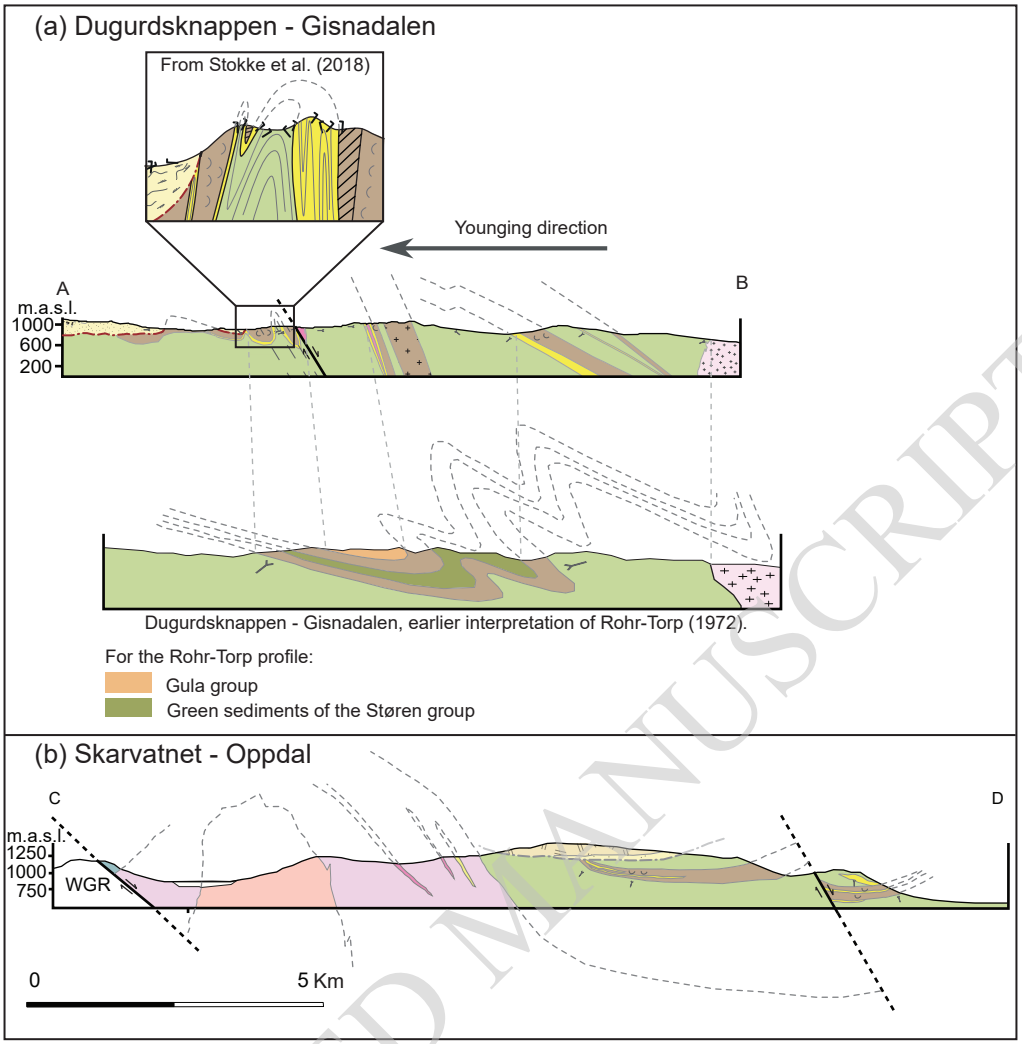

Skuggliberga Unit
- Andesite
- Sandstone, commonly crossbedded

Silurian intrusive
- Innset massif, diorite

Skarvatnet Unit
- Skaret succession
- Storgruvpiken rhyolite
- Kinna volcanic succession

Trollhøtta Unit
- Trachyandesite, trachydacite
- Siltstone and turbiditic sandstone
- Chert and silty chert
- Metabasalt
- Metadolerite

- Unconformity
- Lithological boundary
- Inferred lithological boundary
- Fold axial plane
- Normal fault
- Pillow structure
- Way up indicator